DATA SET CATALOG #54

Explorer 21 & 28

Solar & Galactic Protons

64-060A-03A 3 tapes

65-042A-03A 15 tapes

Table of Contents

---

1. INTRODUCTION:

The documentation for this data set was originally on paper, kept in NSSDC's Data Set Catalogs (DSCs). The paper documentation in the Data Set Catalogs have been made into digital images, and then collected into a single PDF file for each Data Set Catalog. The inventory information in these DSCs is current as of July 1, 2004. This inventory information is now no longer maintained in the DSCs, but is now managed in the inventory part of the NSSDC information system. The information existing in the DSCs is now not needed for locating the data files, but we did not remove that inventory information.

The offline tape datasets have now been migrated from the original magnetic tape to Archival Information Packages (AIP's).

A prior restoration may have been done on data sets, if a requestor of this data set has questions; they should send an inquiry to the request office to see if additional information exists.

2. ERRATA/CHANGE LOG:

NOTE: Changes are made in a text box, and will show up that way when displayed on screen with a PDF reader.

When printing, special settings may be required to make the text box appear on the printed output.

Version	Date	Person	Page	Description of Change
01				
02				

3 LINKS TO RELEVANT INFORMATION IN THE ONLINE NSSDC INFORMATION SYSTEM:

http://nssdc.gsfc.nasa.gov/nmc/

[NOTE: This link will take you to the main page of the NSSDC Master Catalog. There you will be able to perform searches to find additional information]

4. CATALOG MATERIALS:

a. Associated Documents To find associated documents you will need to know the document ID number and then click here. http://nssdcftp.gsfc.nasa.gov/miscellaneous/documents/

b. Core Catalog Materials

IMP-B

RATES & P.H. REDUCED C.R. DATA TAPES

64-060A-03A

THIS DATA SET HAS BEEN RESTORED. ORIGINALLY THERE WERE THREE 7-TRACK, 556 BPI TAPES, WRITTEN IN BINARY. THERE IS ONE RESTORED TAPE. THE DR TAPE IS A 3480 CARTRIDGE AND THE DS TAPE IS 9-TRACK, 6250 BPI. THE ORIGINAL TAPES WERE CREATED ON AN IBM 7094 COMPUTER. THE DR AND DS NUMBERS ALONG WITH THE CORRESPONDING D NUMBERS AND TIME SPANS ARE AS FOLLOWS:

DR#	DS#	D#	FILES	TIME SPAN
DR003396	DS003396	D001597	1-2	10/04/64 - 11/30/64
		D001598	3-4	11/29/64 - 01/27/65
		D001599	5-6	01/27/65 - 04/09/65

UNIVERSITY OF CHICAGO DATA FORMATS FOR LIBRARY MAGNETIC TAPES

FROM SATELLITES IMP-I, IMP-II and IMP-III* Explorers 18, 21, 33

C. Y. Fan, G. Gloeckler, L. A. Littleton and J. A. Simpson
Enrico Fermi Institute for Nuclear Studies
University of Chicago
Chicago, Illinois 60637

64-060A-03A

IMP 1 (03)
IMP 2 (03)
IMP 3 (03)

Format in IMP 1 File

Laboratory for Astrophysics and Space Research

Preprint Number
EFINS-66-02

TAPES ARE 556 BPI, BINARY, 7-track, 2 FILES.

64-060A-03A · 3 TAPES

D-1598 C-2241
D-1599 C-2240
D-1599 C-2242

11/29/64 - 1/29/65
10/4/64 - 11/30/65
1/27/65 - 4/4/65

*This work was supported in part by the National Aeronautics and Space Administration under Contract NASA-NAS-5-2990.

65-042A-03A 15 TAPES

UNIVERSITY OF CHICAGO DATA FORMATS FOR LIBRARY MAGNETIC TAPES FROM SATELLITES IMP-I, IMP-II and IMP-III*

C. Y. Fan, G. Gloeckler, L. A. Littleton and J. A. Simpson
Enrico Fermi Institute for Nuclear Studies
University of Chicago
Chicago, Illinois 60637

Introduction

In accordance with NASA policy we have prepared for the use of the scientific community the data we obtained from the satellites IMP-I, IMP-II and IMP-III. The library magnetic tapes have been carefully edited over a period of at least one year and have been turned over to the NASA Data Library for release at times decided by mutual agreement. This document describes the format of the data found on the tapes and describes the relationship of the data words to the physical parameters which we were measuring. A reprint giving the main features of the IMP-I instrument is included with this document as well as a list of our scientific papers published in 1964-1965 which are based on the use of these data.

*This work was supported in part by the National Aeronautics and Space Administration under Contract NASA-NAS-5-2990.

Content:

1. The Data Processing System

The purpose of the data processing system is to produce magnetic tapes containing all the available data in chronological order, with errors either deleted or flagged. These tapes are intended to be in an efficient format for use by data analysis programs.*

The time base used is the Chicago sequence count. (See 4.6 below.) This is an integer which is approximately zero at time of launch, increasing by one for each spacecraft telemetry sequence. Unfortunately, a spacecraft sequence counter, as such, does not have a predictable relationship to real time over the lifetime of the satellite, since the spacecraft may turn off for varying lengths of time due to lack of power. The Chicago sequence count is artificially projected over periods when the spacecraft is off, the intent being to approximate as closely as possible a uniform time base whose unit value is an integral multiple of the time between telemetry readouts of the experiment.

The data processing system has four major parts:**

1) Reformatting the data and generating error flags.

2) Checking and correcting the sequence count, and deleting any large sections of the data which cannot be corrected.

3) Sorting the data.

4) Checking for and deleting errors in the processed data.

---

*Actually there is a fair amount of unused space in the library tapes; this is primarily due to the desirability of retaining (so far as possible) a single tape format throughout the system.

**The Appendix gives a description of the programs involved. Figure 3 shows overall data flow.

Step four may involve reprocessing through steps two and three, depending on the number and seriousness of errors found.

In fact, it is possible that the library tapes produced may not in some cases completely fulfill the specifications of the system. This may be due either to human error, e.g., incorrect generation of a special sequence count correction for a case in which the standard procedures are not satisfactory; or to a decision that the cost (in personnel and machine time) of correcting some small amount of data would be greater than the data is worth.

2. General Description of Tape Format

The tapes are written at 556 BPI in IBM 7090 binary format;i.e., odd parity, 36 bits or six characters per word; standard 7090 BCD code for items in BCD. Physical records are 804 words (4824 characters) in length, divided into six logical records of 134 words each. Each logical record consists of a header of five words, three data blocks of 42 words each, and a trailer of three words. A tape is terminated by an end-of-file. One physical tape normally contains between one and two months of data. (See Figure 1.)

Logical records are sorted according to the Chicago sequence count (See 4.6 below.) of data block No. 1. This results in the data being effectively in increasing time order, although since all available data are included, more than one logical record covering a single time period may be present (if there was coverage by more than one tracking station for that time). A logical record contains all available data for a four spacecraft sequence period (format) from one tracking station. Only three

sequences are present in the record since every fourth sequence contains no Chicago data. These are referred to as sequence number one, sequence number two, and sequence number three.

Words or parts of words not specifically described herein do not necessarily contain zeros.

3. Itemization of Data within a Logical Record

3.1 Header Block — Words 1 - 5 of logical record

Word	Contents
1	EDT Number (4.1)*
2 - 3	Station ID (4.2)
4	Record Flag (4.3)
5	Input Flag 1 (4.4, 4.4.1)

3.2 Data Blocks

3.2.1 Data Block 1 - Words 6 - 47 of logical record. Contains data, if any, from sequence number 1. (4.9)+

3.2.2 Data Block 2 - Words 48 - 89 of logical record. Contains data, if any, from sequence number 2.

3.2.3. Data Block 3 - Words 90 - 131 of logical record. Contains data, if any from sequence number 3.

3.2.4 Itemization of data within any data block.

* See item descriptions in Section 4 below.

+ If the sequence number cannot be determined, the data for the sequence is in data block 1, and data blocks 2 and 3 immediately following contain no data.

Block Word	Contents
1-2	Sequence Time (4.5)
3	Chicago Sequence Count (4.6)
4	GSFC Sequence Count (4.7)
5	Frame Length (4.8)
6	Sequence Flag (4.9)
7	Time Flag (4.10)
8	Input Flag 2 (4.4.2)
9	Input Flag 3 (4.4.3)
10	Input Flag 4 (4.4.4)
11 - 12	Not used
13	S/C Frame 0 - Time (4.11)
14	D1D2D3 Accumulator (4.12, 4.12.3)
15	D1D2 Accumulator (4.12.2)
16	D1D2D3D4 Accumulator (4.12.4)
17	D1 Accumulator (4.12.1)
18	S/C Frame 1 - Time
19	D1 Pulse Height (4.13)
20	D3 Pulse Height
21	A-C/D5 (4.14)
22 - 23	Not used
24	S/C Frame 8 - Time
25	D1D2D3 Accumulator
26	D1D2 Accumulator
27	D1D2D3D4 Accumulator
28	D1 Accumulator
29	S/C Frame 9 - Time
30	D1 Pulse Height
31	D3 Pulse Height
32	A-C/D5
33 - 42	Not used

3.3 Trailer Block - Words 132 - 134 of logical record

Word	Contents
1	Not used
2	Look - Ahead Flag (4.15)
3	Not used

4. Description of Individual Data Items

4.1 EDT Number

Six BCD characters giving the number of the GSFC Experimenter's Data Tape from which these data were taken.

4.2 Station ID

Twelve BCD characters, arranged as follows:

NNMMDDYSSTTT, where

- NN = Satellite Number
- MM = Month
- DD = Day
- Y = Year
- SS = Tracking Station Code
- TTT = Analog Tape Number

4.3 Record Flag

One 36-bit word containing four flags:

(Record Flag) Bit 0

= 0 if data in record.

= 1 if no data.

(Sequence 1 Flag) Bit 23

= 0 if data for Sequence 1 (e.g., in data block 1).

= 1 if no data

(Sequence 2 Flag) Bit 29

= 0 if data for Sequence 2.

= 1 if no data

(Sequence 3 Flag) Bit 35

= 0 if data for Sequence 3.

= 1 if no data.

4.4 Input Flags

An input flag is a nine-bit quantity indicating whether the corresponding data item as received on the EDT was free from obvious errors. If all nine bits are zero, no errors were found; if some bits are one, some error was found. The errors checked for are tape redundancies, missing data, and illegal (non-numeric) characters. If any bit of an input flag is non-zero, the corresponding data item does not contain any meaningful information.

4.4.1 Input Flag 1

One word containing two input flags:

(Station ID Input Flag 1) Bits 0 - 8

Input flag for Word No. 1 of Station ID.

(Station ID input Flag 2) Bits 9 - 17

Input flag for Word No. 2 of Station ID.

4.4.2 Input Flag 2

One word containing four input flags:

(Sequence Time Input Flag 1) Bits 0 - 8

Input flag for first word of sequence time.

(Sequence Time Input Flag 2) Bits 9 - 17

Input flag for second word of sequence time.

(Sequence Count Input Flag) Bits 18 - 26

Input flag for GSFC sequence count.

(Frame 0 Time Input Flag) Bits 27 - 35

Input flag for frame 0 time.

4.4.3 Input Flag 3

One word containing two input flags:

(Frame 1 Time Input Flag) Bits 0 - 9

Input flag for frame 1 time.

(Frame 8 Time Input Flag) Bits 27 - 35

Input flag for frame 8 time.

4.4.4 Input Flag 4

One word containing one input flag:

(Frame 9 Time Input Flag) Bits 0 - 8

Input flag for frame 9 time.

4.5 Sequence Time

Twelve BCD characters giving the beginning time for the spacecraft sequence as follows:

DDDHHMMSSMMM, where

DDD = day of year

HH = hour

MM = minute

SS = second

MMM = millisecond

4.6 Chicago Sequence Count

One word containing a flag and the Chicago sequence count value: The Chicago sequence count is constructed by the Chicago data processing programs from the GSFC sequence count, the sequence number, the frame length, and the time. It increases by one for each spacecraft sequence (or by one for the time required for one sequence if the satellite is turned off) and does not recycle. (Maximum value is $2^{22}-1$, which would allow a satellite life of approximately ten years.)

(Sequence Count Correction Flag): Bit 0 Sign

= $\bar{1}$ if, and only if, the Chicago and GSFC sequence counts differ by other than the rescaling factor (for the GSFC sequence count).

(Chicago Sequence Count) Bits 13-35

Chicago sequence count in binary integer form.

4.7 GSFC Sequence Count

Six BCD characters giving the GSFC sequence count. (The GSFC sequence count is constructed by the Goddard Space Flight Center data processing programs from the satellite clock reading, and should increase by one for each spacecraft sequence, recycling after 99999.) Discussed by White (1964b).

4.8 Frame Length

One word containing the frame length input flag and the frame length:

(Frame Length Input Flag) Bits 0-8

The input flag for the frame length.

(Frame Length) Bits 9-35

Spacecraft frame length in milliseconds

in binary integer form.

4.9 Sequence Flag

One word containing two flags and the sequence number:

Chicago data is read out twice per spacecraft sequence for three successive sequences and not at all during the fourth. (See Table 2.)

The Sequence Number is 1, 2, 3 for the three successive sequences in which readouts occur, and four for the sequence with no readout. The sequence number is not included on the Chicago EDT, but computed by the Chicago data processing programs. The generated sequence number is set to four if the actual sequence number cannot be determined.

(Data Flag) Bits 22-23

= 0 if and only if all input flags are zero for Chicago data (contained in data block words 14-17, 19-21, 25-28, 30-32) for this sequence.

= 1 if some but not all imput flags for Chicago data for this sequence are non-zero.

= 2 only if all input flags for Chicago data for this sequence are non-zero

(Sequence Number Flag) Bit 29

= 0 if the sequence number is reliable.

= 1 if the sequence number is questionable or not determinable.

(Sequence Number) Bits 33-35

The sequence number in binary integer form.

4.10 Time Flag

One word containing six flags:

(ET Flag Input Flag) Bits 0 - 7

The input flag for the ET flag. (Note that this is only 8 bits.)

(ET Flag Discrepancy Flag) Bit 8

= 1 if and only if all ET flags on the EDT for this sequence were not identical.

(Time Flag) Bits 9 - 17

= 0 if and only if time, GSFC sequence count and sequence number are consistent.

The time flag indicates the degree of consistency within one EDT of the time, GSFC sequence count, and (computed) sequence number. Individual bits are set as follows:

Bit 17 = 1 if time and GSFC sequence count are inconsistent.

16 = 1 if the time to GSFC sequence count consistency relation is re-initialized.

15 = 1 if the GSFC sequence count is inconsistent with the time and sequence number.

14 = 1 if the time is less than a previous time within the same acquisition. (An acquisition is defined by the station and analog tape numbers of the station ID.)

Bit 13 = 1 if the GSFC sequence count is less than a previous sequence count of the same acquisition.

12 = 1 if the time or GSFC sequence count previous maximum within an acquisition is re-initialized.

11 = 1 if the time is inconsistent with the (computed) sequence number.

10 = 1 if the GSFC sequence count is inconsistent with the sequence number.

9 = 1 if the time or GSFC sequence count to sequence number consistency relation is re-initialized.

(Time Summary Flag) Bits 18 - 23

The time summary flag is constructed using the same criteria as the time flag and will normally be a shortened version of the time flag.

= 0 if and only if both time and GSFC sequence count are apparently reliable.

= 1 if only time is apparently reliable.

= 2 if only GSFC sequence count is apparently reliable.

= 3 if time is questionable but appears more reliable than GSFC sequence count.

= 4 if GSFC sequence count is questionable, but appears more reliable than time.

= 5 if no consistency can be found.

(ID Time Flag) Bits 24-29

The ID time flag indicates whether the date given in the station ID is reliable.

= 0 if and only if the ID date appears to be reliable.

= 1 if the ID date disagrees with the spacecraft frame 0 time.

= 2 if the ID date is not within the life of the satellite.

= 4 if the ID date is impossible (not a legal date in the calendar).

(ET Flag) Bits 30-35 (White, 1964a)

The GSFC ET flag in binary integer form encoded as follows:

GSFC	Chicago Code
0	0
2	1
4	2
6	4
8	8
1	32
3	33
5	34
7	36
9	40

4.11 Time

Time in milliseconds of the year, as a 36-bit binary integer. The first of January is day 1; the time in milliseconds for 0000:00.00 Jan. 1 is 86400000. (The frame times indicate the GMT time at the beginning of the spacecraft frame. Note that Chicago data readout does not occur at the beginning of the frame - see

Table 3).

4.12 Accumulator

One word containing an accumulator reading and the associated input flag. This is a spacecraft accumulator readout containing a Chicago count rate output. The accumulator may or may not be reset after readout, as indicated. The accumulator length and the amount of pre-scaling included in the Chicago package are also given below. (See also Table 4.)

(Accumulator x Input Flag) Bits 0 - 8

The input flag for this accumulator readout.

(Accumulator x Reading) Bits 9 - 35

The accumulator reading in binary integer form.

('x' is D1, D1D2, D1D2D3, or D1D2D3D4.)

The four accumulators are:

4.12.1 (D1 Accumulator)

Spacecraft word 7b = 12 bits

Prescale factor = 64

Accumulated D1 counts

Not reset

4.12.2 (D1D2 Accumulator)

Spacecraft word 4b = 9 bits

Prescale factor = 16

IMP-I: Accumulated D1D2 counts

Reset

IMP-II, III: Accumulated $D1D2\overline{D3}$ counts

Not reset

4.12.3 (D1D2D3 Accumulator)

Spacecraft word 4a = 6 bits

Prescale factor = 4

IMP-I: Accumulated D1D2D3 counts

Reset

IMP-II, III: Accumulated D1D2D3$\overline{D4}$ counts

Not reset

4.12.4 (D1D2D3D4 Accumulator)

Spacecraft word 7a = 3 bits

Prescale factor = 8

Accumulated D1D2D3D4 counts.

Not reset

4.13 Pulse Height

One word containing two input flags, the Chicago pulse height analyzer range, and the Chicago pulse height analyzer channel for the D1 or D3 pulse height analyzer:

(Pulse Height $\underline{x}$ Input Flag) Bits 0 - 8
Input flag for this pulse height.

(Range $\underline{x}$ Input Flag) Bits 9 - 17
Input flag for this range.

(Range $\underline{x}$) Bit 29
= 0 if range = low.
= 1 if range = high.*

*Low range indicates high gain amplifier; high range indicates low gain amplifier.

(Pulse Height x) Bits 30 - 35

Pulse height analyzer channel reading in binary integer form.

('x' is either D1 or D3).

4.14 A-C/D5

One word containing an input flag and the anti-coincidence or D5 readout:

(A-C/D5 input Flag) Bits 0 - 8

Input flag for the anti-coincidence or D5 readout.

(A-C/D5) Bit 35 -

IMP-I: Chicago pulse height analyzer anti-coincidence bit:

= 0 if no anti-coincidence.

= 1 if anti-coincidence.

IMP-II,III: The reading of the Chicago D5 accumulator:

1 bit

Prescale factor = 64

IMP-II: Not reset

IMP-III: Reset

4.15 Look-Ahead Flag:

One word containing one flag:

Bit 24 = 0 if more records covering same time period (i.e., with same Chicago sequence count for sequence number 1) follow this one.

= 1 if this is the last (or only) data for this period.

5. Relationship of Physical Parameters to Data Items and Data Block Words.

In order to clarify the connection between the preceding data description and publications referring to the data, the following explanation is given. The description is based on the IMP-I experiment. IMP-II and IMP-III are basically similar; differences are indicated where appropriate.

The instrument is a four-detector charged particle telescope, as shown in Figure 2. The first two elements are gold-silicon surface barrier detectors (called D1 and D2 respectively) with an energy threshold of 180 kev, a surface area of 3.5 cm^2, and depletion depth of 200 microns (on IMP-III these are lithium drifted detectors with surface area of 5.7 cm^2 and depletion depth of 900 microns). The third detector (D3) is a CsI (Tl) crystal whose light output is detected by two gold-silicon surface barrier photodiodes mounted on opposite sides of the crystal. D4, a plastic scintillator cup around D3, is coupled to a photomultiplier tube by a light-scattering chamber. The geometrical factor of D1 is approximately 8 cm^2 ster. (IMP-III: 12 cm^2 ster.). The geometrical factor of the telescope is 0.85 cm^2 ster. (IMP-III: 1.2 cm^2 ster.). The main axis of the telescope is normal to the spin axis of the satellite.

IMP-II and IMP-III have in addition to the main telescope a separate gold-silicon surface barrier detector called D5, of 0.1 cm^2 surface area and 50 micron depletion depth, whose orientation is the same as that of the detectors in the telescope.

An aluminized mylar window in front of the telescope sets a lower energy limit for the detection of charged particles. D1 is sensitive to electrons with energies greater than 180 kev, to 0.9 to 190 Mev protons, and to particles with charge of two or greater and having energies greater than a few Mev/nucleon. D1 also detects electrons with energy greater than 30 kev which "pile-up" within the resolving time of the instrument. Vertically incident 6.5 to 190 Mev protons cause D1D2 coincidence, while D1D2D3 requires proton energies over 19 Mev and D1D2D3D4 over 90 Mev. The telescope detects heavier particles ($Z \leq 6$) having energies greater than a few Mev/nucleon. The particle energy ranges are slightly different for IMP-III. D5 detects mainly low energy protons; the electron sensitivity is relatively low because of the small depletion depth.

Table 1 gives the correspondence between the IMP-I data names and their places in the logical record, while Table 4 shows the differences between the data outputs of IMP-I, IMP-II and IMP-III.

5.1. Rate Analysis

The counting rate outputs from the experiment are D1, D1D2 coincidence (IMP-II, III: $D1D2\overline{D3}$ coincidence), D1D2D3 coincidence (IMP-II, III: $D1D2D3\overline{D4}$ coincidence), and D1D2D3D4 coincidence. (IMP-II and IMP-III also have an output from D5). All rate outputs are pre-scaled within the instrument,

so the number of events indicated by the spacecraft accumulator readouts must be multiplied by the appropriate scaling factor. (See 4.12) A vertically incident 50 Mev proton, for example, will penetrate the D1, D2 and D3 detectors (but not D4), and contribute one count to each of the D1, D1D2, and D1D2D3 unscaled rates (IMP-II, III: to the D1 and D1D2D3$\overline{D4}$ rates). Sixty-four such events will increment the spacecraft D1 accumulator by one, the D1D2 accumulator by four (IMP-I only), and the D1D2D3 accumulator by sixteen.

Rates in counts/sec may be computed by:

$$R = \frac{K(A_n - (A_{n-1}B))}{LB(16(S_n - S_{n-1}) + F_n - F_{n-1} - 5/16) + L(1-B)(8 - 5/16)}$$

where:

A is the accumulator readout

K is the scaling factor

S is the sequence count

F is the frame

L is the frame length in seconds (nominally 5.120)

B = 1 if the accumulator is not reset

B = 0 if the accumulator is reset

and 5L/16 is the dead time of the accumulators during readout.*

*It is assumed that the spacecraft accumulator under consideration has not recycled between A_{n-1} and A_n.

5.2 Pulse Height Analysis

The instrument includes two 64-channel pulse height analyzers, one connected to D1 and one to D3. The first D1D2 or D1D2D3 coincidence after a telemetry readout causes pulse height analysis to occur: D1 analysis only for D1D2$\overline{D3}$, coincidence, D1 and D3 analysis for D1D2D3 coincidence. Analysis of a D1D2D3D4 coincidence event sets the A-C bit to one on IMP-I. IMP-II and IMP-III only analyze events which do not trigger D4; the A-C bit is used for the D5 detector rate readout. The analysis is stored until the next telemetry readout, with no other being allowed until that time. Since of the many events which may occur in a sequence (approximately 82 seconds), only two can be pulse height analyzed, the pulse height analysis only samples the charge, mass, and energy distribution of the incoming flux.

In order to extend the dynamic range of the pulse height analyzers while retaining good resolution, an electronic range switch is incorporated in each. The switch determines which of two possible amplifications is needed for a given pulse. If a particle produces a large pulse so that low amplification is needed, the appropriate "HI/LO RANGE" switch is set to one and the "range" is called high.

For a particle penetrating past D1, the "D1PHA" measures the fraction of energy lost (dE/dx) in D1, which depends inversely on the particle's total energy. For a particle which stops in D3, the "D3PHA" measures total residual kinetic energy (E). In this case E, dE/dx, Z(charge), and A (mass) are uniquely related.

Table 5 gives the pulse height analyzer calibrations.

UNIVERSITY OF CHICAGO IMP-I EXPERIMENT LOGIC OUTPUTS WITHIN TAPE FORMAT

Output*	Data Item**	Data Block Words	Bits
D_1HI/LO RANGE	D1 Pulse Height (Range D1)***	19,30	(29)
D_1PHA	D1 Pulse Height (Pulse Height D1)	19,30	(30-35)
D_1RATE	D1 Accumulator	17,28	(9-35)
D_1D_2 RATE	D1D2 Accumulator	15,26	(9-35)
D_3HI/LO RANGE	D3 Pulse Height (Range D3)***	20,31	(29)
D_3PHA	D3 Pulse Height (Pulse Height D3)	20,31	(30-35)
$D_1D_2D_3$ RATE	D1D2D3 Accumulator	14,25	(9-35)
$D_1D_2D_3D_4$ RATE	D1D2D3D4 Accumulator	16,27	(9-35)
AC ON/OFF	A-C/D5	21,32	(35)

*Fan, et al. (1965), Figure 3.

**Item names used in this paper.

***Note that pulse height analysis with high gain preamplification is here referred to as being low range; low gain preamplification as high range.

Table 1

FOUR SEQUENCE TELEMETRY FORMAT

Sequence Count	Sequence Number	Chicago Data Transmitted?
k	1	Yes
k+1	2	Yes
k+2	3	Yes
k+3	4	No
k+4	1	Yes
k+5	2	Yes
k+6	3	Yes
k+7	4	No

Table 2

SINGLE SEQUENCE TELEMETRY FORMAT

SINGLE SEQUENCE TELEMETRY FORMAT

Frame	Channel	S/C Word	S/C Accum.	No. of Bits:	Data Item
0	6-10	4	4a	6	D1D2D3 accumulator
			4b	9	D1D2 accumulator
0	11-15	7	7a	3	D1D2D3D4 accumulator
			7b	32	D1 accumulator
1	11-15	8		15	D1 pulse height(and range bit), D3 pulse height, A-C/D5
8	6-10	4	4a	6	D1D2D3 accumulator
			4b	9	D1D2 accumulator
8	11-15	7	7a	3	D1D2D3D4 accumulator
			7b	12	D1 accumulator
9	11-15	8		15	D1 pulse height, D3 pulse height, A-C/D5

One channel = 0.32 sec.

One frame = 5.12 sec. = 16 channels

One sequence = 81.92 sec. = 16 frames

S/C (spacecraft) words are "frozen" during readout.

$$2\overline{)81.92}\quad 40.96$$

Table 3

Avg. bit rate $\frac{45}{54.6} \approx 0.82$ b.d./second

$40.96 \times \frac{4}{3} = 54.6$ sec. Re words read out period

IMP-I, IMP-II and IMP-III Data Outputs

Data Item	No. of Bits	IMP-I	IMP-II	IMP-III
1. D1 Accumulator	12	D_1 Rate	D_1 Rate	D_1 Rate
Prescale		64	64	64
Reset?		No	No	No
2. D1D2 Accumulator	9	D_1D_2 Rate	$D_1D_2\overline{D_3}$ Rate	$D_1D_2\overline{D_3}$ Rate
Prescale		16	16	16
Reset?		Yes	No	No
3. D1D2D3 Accumulator	6	$D_1D_2D_3$ Rate	$D_1D_2D_3\overline{D_4}$ Rate	$D_1D_2D_3\overline{D_4}$ Rate
Prescale		4	4	4
Reset?		Yes	No	No
4. D1D2D3D4 Accumulator	3	$D_1D_2D_3D_4$ Rate	$D_1D_2D_3D_4$ Rate	$D_1D_2D_3D_4$ Rate
Prescale		8	8	8
Reset?		No	No	No
5. D1 Pulse Height	6	D_1 PHA	D_1 PHA	D_1 PHA
6. D1 Range	1	D_1 Range	D_1 Range	D_1 Range
7. D3 Pulse Height	6	D_3 PHA	D_3 PHA	D_3 PHA
8. D3 Range	1	D_3 Range	D_3 Range	D_3 Range
9. A-C/D5	1	AC	D_5 Rate	D_5 Rate
Prescale		n.a.	64	64
Reset?		n.a.	No	Yes

Table 4

IMP - I,II,III Pulse Height Analysis Calibration
Channel Thresholds in Millivolts

Channel	IMP - I Thresholds				IMP - II Thresholds				IMP - III Thresholds			
	D1		DJ		D1		DJ		D1		DJ	
	L*	H*	L	H	L	H	L	H	L	H	L	H
1			2.0									
2	1.3		2.3						1.30			
3	1.35		2.58						1.91			
4	1.5		2.98				2.0		2.45		0.59	
5									3.54	55.3	0.71	
6	2.08		4.08			16.5			4.7	59.3	0.98	
7										70.4	1.2	
8	2.9	30.1	5.25					21.0	7.6	82.6	1.39	
9										9[illegible]	1.63	12.1
10	3.8	43.4	5.4		2.5	35	4.6	28.0	9.2	11[illegible]	1.89	14.1
11				35.8								15.7
12	4.75	58.9	7.52	36.7					11.5		2.39	17.4
13												18.9
14	5.7	75.1	8.7	44.3						170	2.86	20.5
15												
16	6.72	92.9	9.82	51.4						195	3.33	23.8
17												
18	7.72	109	10.8	58.4					17.3	225	3.77	27.0
19												
20	8.8	126	11.4	65.3	5.2	75	8.1	52		252		30.1
21												
22	9.85	143	13.0	72.1					21.5	264	4.76	33.4
23												
24	10.4	161	14.1									36.5
25												
26	11.5	178	15.3	85.7					25.7	351	5.63	39.9
27												
28	12.5	196	16.3	92.7								
29												
30	13.5	213	17.5	100	7.9	120	11.6	75	29.7	419	6.53	45.8
31												
32	14.6	233	18.7	108								48.9
33												
34	15.7	250	19.9	115					34.0	488	7.39	52.0
35												
36	16.7	268	21.1	120							7.88	
37												
38	17.9	285	22.2	128					37.6	542	8.33	58.0
39												
40	18.9	303	23.5	135	10.6	166	15.0	97				
41												
42	19.9	323	24.7	143					41.8	611	9.22	64.0
43												
44	21.1	342	26.0	151								
45												
46	22.2	361	27.3	158					46.0	680	10.0	70.3
47												
48	23.4	381	28.6	166								
49												
50	24.5	400	30.0	174	[illegible]	213	18.5	120	50.0	748	10.8	76.6
51												
52	25.7	419	31.3	182	[illegible]				51.7			
53									52.9			
54	26.9	441	33.0	190					53.4	815	11.7	83.0
55									54.4		11.89	84.4
56	28.2	460	34.5	198			20.5				12.1	85.9
57	28.9		35.3									87.9
58		480		208	[illegible]			200		88[illegible]		
59						[illegible]				898		
60		503		218								
61		513		227								
62		583										
63												

+ IMP - II figures are not threshold voltages.
* 'L' indicates low range; 'H' indicates high range.

Table 5

References

Fan, C. Y., G. Gloeckler, K. C. Hsieh and J. A. Simpson, The isotopic abundances and energy spectra of He^3 and He^4 above 40 Mev per nucleon from the galaxy, (to be published) 1966. (IMP-III)

Fan, C. Y., G. Gloeckler and J. A. Simpson, Initial results from the first interplanetary monitoring platform (IMP-I), Trans. Am. Geophys. Union, 45(3), 507-509, 1964a.

Fan, C. Y., G. Gloeckler and J. A. Simpson, Evidence for >30 kev electrons accelerated in the shock transition region beyond the earth's magnetospheric boundary, Phys. Rev. Lett., 13, 149-153, 1964b. (IMP-I)

Fan, C. Y., G. Gloeckler and J. A. Simpson, Cosmic radiation helium spectrum below 90 Mev per nucleon measured on the IMP-I satellite, J. Geophys. Res., 70, 3515-3527, 1965.

Fan, C. Y., G. Gloeckler and J. A. Simpson, Solar modulation of the galactic helium spectrum above 30 Mev per nucleon, Proceedings of the International Conference on Cosmic Rays, London, Physical Society, London, (to be published March, 1966) 1966a.

Fan, C. Y., G. Gloeckler and J. A. Simpson, Acceleration of particles in the earth's shock transition region and beyond, ibid, 1966b.

Fan, C. Y., G. Gloeckler and J. A. Simpson, Protons and helium nuclei within interplanetary magnetic regions which co-rotate with the sun, ibid., 1966c.

Fan, C. Y., G. Gloeckler and J. A. Simpson, Acceleration of electrons near the earth's bow shock and beyond, J. Geophys. Res., (to be published April 1, 1966) 1966d.

Gloeckler, George, Solar modulation of the low-energy galactic helium spectrum as observed on the IMP-I satellite, J. Geophys. Res., 70, 5333-5343, 1965.

Ness, Norman F., IMP Information Processing, NASA-GSFC, Greenbelt, Maryland, 1962.

White, Hosea, D., IMP PFM Encoder, Code 631.1, NASA-GSFC, Greenbelt, Maryland, 1962.

White, Hosea D., Significance of the ET Flag in the S-74 (IMP) Information Processing System, Code 612, NASA-GSFC, Greenbelt, Maryland, 1964a.

White, Hosea D., Use of a Satellite Clock in PFM Telemetry Systems, Code 612, NASA-GSFC, Greenbelt, Maryland, 1964b.

8. Appendix . - Description of Computer Programs

The programs are written for the IBM 7094 and SDS 910 computers,* and are in general rather specialized, making use of the particular hardware and software configurations of the computing systems used.

8.1 Reformatting and Generating Error Flags.

8.1.1 IMPFT - 7094 FAP program and subroutines.

IMPFT uses as input the experimenter's data tape supplied by NASA-GSFC. The data, time, and sequence count are checked for errors, and an output tape is produced containing the input data converted into 7094 binary integer format, together with error flags as appropriate.

8.1.2 CHEAQ - 7094 FORTRAN program with FORTRAN and FAP subroutines.

CHEAQ is used to selectively check experiment performance and data quality.

CHEAQ uses the IMPFT output tape for input, producing printed output consisting of:

1) Spacecraft and Chicago experiment data.
2) Input error flags.
3) Computed count rates.
4) Pulse height distributions.

*More detailed documentation may be obtained from L. Littleton.

8.2 Checking and Correcting Sequence Count; Deleting Contiguous Sections of Bad Data.

8.2.1 PSEQ - 910 FORTRAN program with Symbol subroutines.

PSEQ projects the sequence count from the data already processed for the satellite, using time, sequence count, and spacecraft telemetry frame length from the previous data and the above plus sequence number from the present data.

Input to PSEQ consists of a time summary card (made up from previous processing) and the IMPFT output tape. PSEQ output is a tape containing projected sequence count corrections and a listing of error conditions, if any.

8.2.2 FTD+C - 910 Symbol program.

FTD+C corrects the sequence count as required, does minor reformatting of the data, deletes any four-sequence (three of which would contain Chicago readouts) blocks in which there is no good Chicago data, and deletes files of data as requested. (At this stage in the processing, a file consists of the data from one tracking station analog tape; in some cases an entire file may be invalid).

Input to FTD+C consists of the IMPFT output tape(s), the PSEQ output tape(s), sequence count correction cards for special cases, and file deletion cards if required. Output is a single tape in slightly altered format.

8.3 Sorting the Data.

8.3.1 SORT - 910 Symbol program.

SORT sorts and merges the data into ascending (Chicago) sequence count order.

Input to SORT is either a single FTD+C output tape, or two previously sorted tapes (to be merged). Output is a single sorted tape, in library tape format.

8.4 Checking for and Deleting Errors.

8.4.1 CLIBE - 7094 FAP program.

CLIBE checks for inconsistency or incorrect order in the sequence count, and for data disagreement within sections of overlapped data (i.e., during times of coverage by more than one tracking station). CLIBE also checks for parity and format errors on the tape.

Input to CLIBE is the SORT output tape. Output is a printed listing of all errors found.

8.4.2 PIULT - 910 Symbol program.

PIULT prints selected sections of the SORT output tape, as required for error checking.

8.4.3 IMPRID - 910 Symbol program.

IMPRID deletes logical records from the SORT output tape, and is used when an isolated record is found to be in error.

Input to IMPRID consists of the SORT (or previous IMPRID) output tape and record deletion cards. Output is another tape in the same format, with the required records deleted.

Captions for Figures

Figure 1. Library tape structure.

Figure 2. Cross-section view of the detector elements and absorbers for the IMP-I and IMP-II cosmic-ray telescopes.

Figure 3. IMP data flow. Only processing which is done at the University of Chicago is shown.

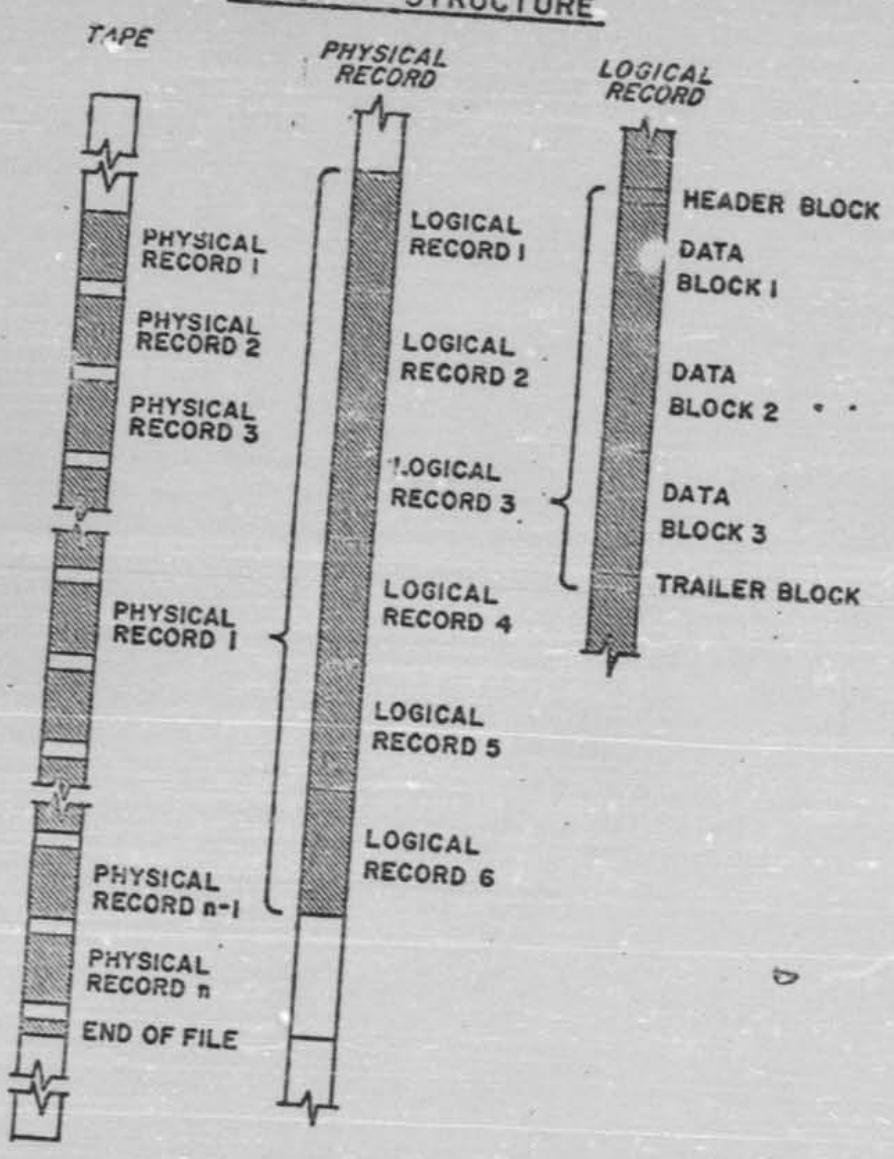
TAPE STRUCTURE
TAPE
PHYSICAL RECORD
LOGICAL RECORD
PHYSICAL RECORD 1
PHYSICAL RECORD 2
PHYSICAL RECORD 3
PHYSICAL RECORD 1
PHYSICAL RECORD n-1
PHYSICAL RECORD n
END OF FILE
LOGICAL RECORD 1
LOGICAL RECORD 2
LOGICAL RECORD 3
LOGICAL RECORD 4
LOGICAL RECORD 5
LOGICAL RECORD 6
HEADER BLOCK
DATA BLOCK 1
DATA BLOCK 2
DATA BLOCK 3
TRAILER BLOCK

Figure 1

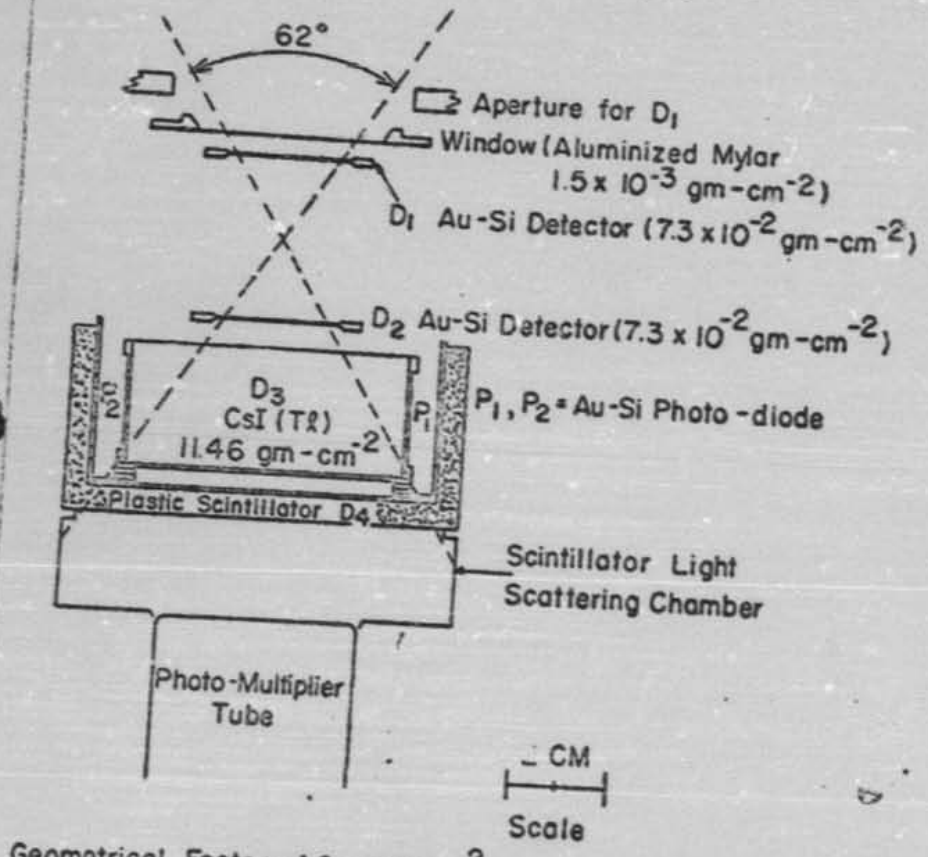

Geometrical Factor = $A\Omega = 0.83$ cm^2-sr.

Fig. 2

IMP DATA FLOW

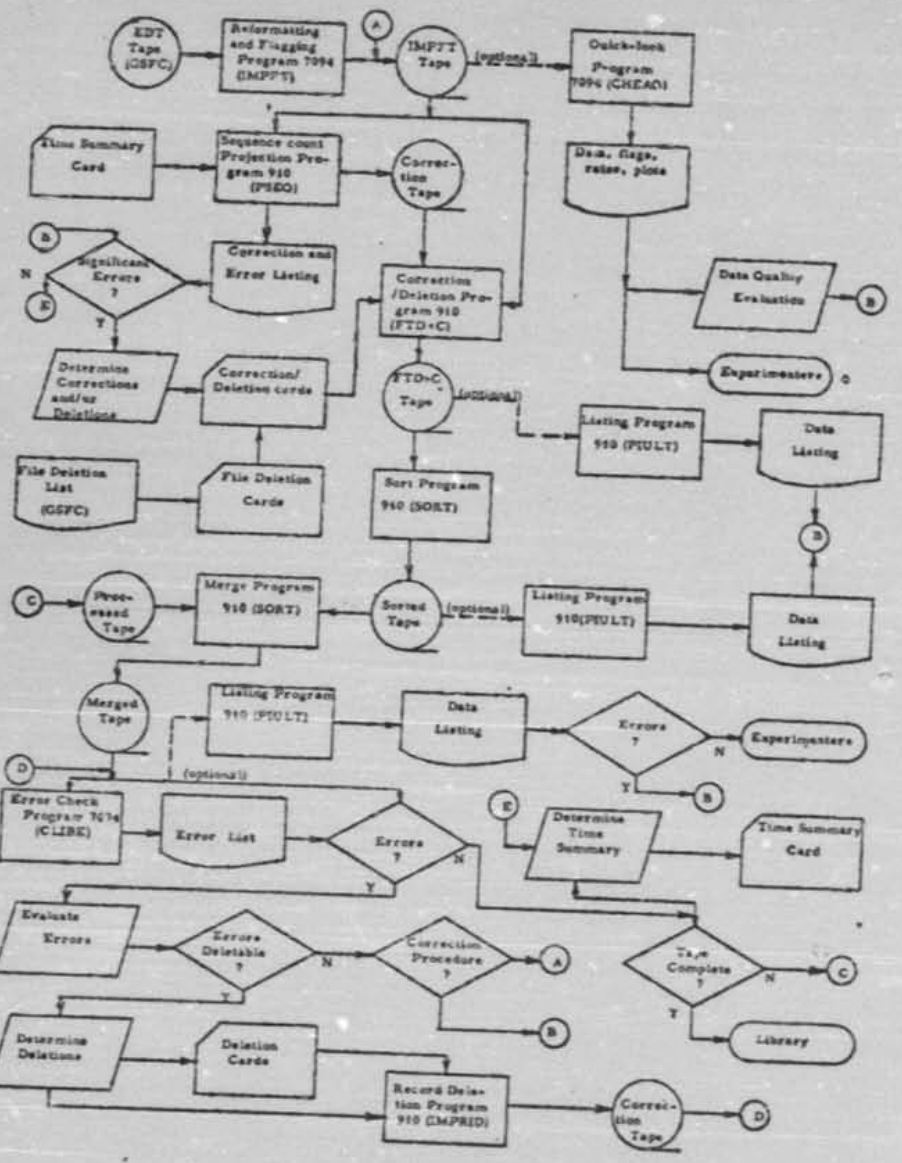

Figure 3.

Journal of
GEOPHYSICAL RESEARCH

VOLUME 70 AUGUST 1, 1965 No. 15

Cosmic Radiation Helium Spectrum below 90 Mev per Nucleon Measured on Imp 1 Satellite

C. Y. FAN

Enrico Fermi Institute for Nuclear Studies

GEORGE GLOECKLER[1] AND J. A. SIMPSON

Enrico Fermi Institute for Nuclear Studies and Department of Physics
University of Chicago, Chicago, Illinois

Abstract. The differential spectrum of primary helium nuclei has been measured over the energy range 30 to 90 Mev per nucleon in six energy intervals. The results are well-represented by the power spectrum

$$dJ/dE = 1.15 \times 10^{-2} E^{-2.62 \pm 0.2} \text{ [cm}^2 \text{ sec ster Mev]}^{-1}$$

where J is the integral flux of He^4 and He^3, and E is the total kinetic energy. This is the time-averaged spectrum from November 27, 1963, to May 1, 1964, near the minimum of the solar activity cycle. There is evidence that this helium spectrum is the low-energy extension of the modulated, interstellar spectrum of cosmic-ray helium: (1) the helium nuclei were continuously present over the 5-month period and not correlated with solar-flare phenomena; (2) this helium spectrum extends smoothly into the higher-energy spectrum for cosmic-ray helium measured in balloons by others in 1962 and known to be of galactic origin; (3) during this period the helium flux increased approximately 35% while the higher-energy cosmic radiation increased ~6%; this is the expected qualitative behavior for the solar modulation of an interstellar spectrum of helium during the decay phase of the interplanetary magnetic fields. Since the Imp 1 (Explorer 18) satellite had an apogee of 198,000 km, primary helium measurements were obtained over most of the orbital period. The experimental apparatus consisted of a solid-state, charged-particle telescope which measured the energy loss and total energy of protons, helium, and some components of higher charge. The novel use of semiconductor detectors, and their dynamic range, energy resolution, stability, and linearity as a function of particle charge, are discussed.

1. INTRODUCTION

In this paper we report the measurement of the primary helium spectrum and flux in the energy range 30 to 90 Mev/nucleon, which is below previous observations. We conclude that these nuclei are of galactic origin; i.e., the galactic spectrum contains helium nuclei with energies down to 30 Mev/nucleon or lower. These nonrelativistic particles are able to reach the vicinity of the earth during periods at the minimums of the 11-year solar activity cycle, at which time the modulation of the galactic cosmic radiation by interplanetary magnetic fields is greatly reduced. Although our measurements cover a period near the solar minimum of 1963–1964, we find that the measured spectrum is being modulated. Clearly, investigations within

[1] National Aeronautics and Space Administration predoctoral fellow.

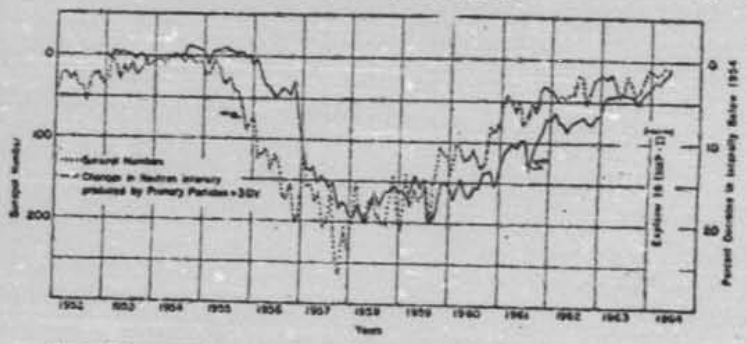

Fig. 1. The 11-year solar modulation of cosmic radiation—principally the proton component—as reflected in the changes of neutron monitor intensity. The variation shown above for the Climax neutron monitor of the University of Chicago corresponds to ~45% change in integral proton intensity above 2.8 Gv.

this restricted time window, and at very low energies, are of importance for attacking two inseparably related problems. One concerns the physical description of the 11-year solar modulation of charged particles from the galaxy. The second is the determination of the low-energy spectrums, flux, and chemical composition of the cosmic radiations outside our solar system—information essential to an understanding of the injection, acceleration, and propagation of galactic cosmic rays.

With regard to the first problem, it has been shown that the inverse relationship between solar activity and ion chamber intensity over 11 years found by *Forbush* [1958] is explained by galactic cosmic rays undergoing modulation mainly beyond the earth's orbit [*Fan, Meyer, and Simpson, 1960*] in a roughly heliocentric, magnetic field transition region [*Simpson, 1964*] whose characteristics are determined mainly by the solar wind [*Parker, 1963*]. In Figure 1 we show the observed changes in neutron monitor intensity over the solar activity cycle which correspond to a change of >45% in the integral primary cosmic ray flux above 3 Gv magnetic rigidity. Direct measurements of proton and helium spectrums above 1 Gv during the solar cycle [*McDonald and Webber, 1962*] indicate that the proton and α spectral forms are indistinguishable either as functions of rigidity or of energy per nucleon. These results and the results mentioned earlier suggest that it is not possible to analyze fruitfully the high-energy spectrums for differences in the effects of modulation upon the proton and helium components. However, in the nonrelativistic range for a given magnetic rigidity (momentum per unit charge), the protons (mass number A to charge number Z ratio equals $A/Z = 1$) have approximately twice the velocity of the helium nuclei ($A/Z = 2$). The consequences of modulation by outward convection may be investigated as well as modulation by inward diffusion. Indeed, a separation or 'splitting' of the proton and helium spectrums based on magnetic rigidity dependence below 2 Gv rigidity has been detected by *Fichtel, Guss, Knifen, and Neelakantan* [1964] and confirmed by later measurements down to ~0.8 Gv for helium [*Ormes and Webber, 1964; Freier and Waddington, 1964; Fichtel, Guss, Stevenson, and Waddington, 1964; Balasubrahmanyan and McDonald, 1964*]. Preliminary results on the helium spectrum measured on Imp 1 (Explorer 18) verify that this effect extends below 0.4 Gv [*Fan et al., 1964a*]. Comparison of these results with the proton spectrum measured on the Imp 1 satellite [*McDonald and Ludwig, 1964*] shows that the spectral differences are greatest at the lowest energies.

With respect to the problem of determining the unmodulated spectrums of protons and helium nuclei in the nearby interstellar space, it is not valid to assume that the galactic spectrums of the different components have the same rigidity dependence or that modulation ceases for the nonrelativistic nuclei at any time during solar activity minimum [*Simpson*, 1964]. Hence, to distinguish spectral differences arising from modulation from differences in the galactic spectrums we are also attempting to study in a series of satellite measurements the relative differences with time of the spectrums for the low-energy proton, helium, and heavier nuclei down to ~10 Mev/nucleon, and to extrapolate these results to obtain a close approximation to the unmodulated spectrums.

These studies require measurements in a satellite free from the cutoff effects of the terrestrial magnetosphere for a time interval of several months at or near solar minimum activity. These requirements were met with the Imp 1 (Explorer 18) satellite, which provided data over the period November 27, 1963, through May 30, 1964, under the solar and modulation conditions shown in Figure 1.

The most suitable parameters for measurement and identification of particles below ~100 Mev/nucleon are particle energy loss ($-dE/dx$), total kinetic energy (E), and/or particle residual range. We have devised an instrument to measure these parameters which is capable of identifying protons, helium, and some components of higher charge number. Since we use the results of the measurements here and in later papers, and since the instrument is novel in its use of semiconductor detectors, its salient characteristics are discussed in section 2.

2. The Experiment

In Figure 2 we have drawn to scale a cross-section view of the charged-particle telescope detector elements. D_1 and D_2 are two gold-silicon surface-barrier detectors of 3.5 cm² sensitive area and silicon thickness of 300 microns. The depletion depths are 200 microns. Since these detectors are photosensitive we use an aluminized Mylar window to eliminate sunlight. The window sets the low energy limit of 0.9 Mev for protons. Thus, vertically incident protons or helium with energies in excess of 6.5 Mev/nucleon produce a coincidence pulse from

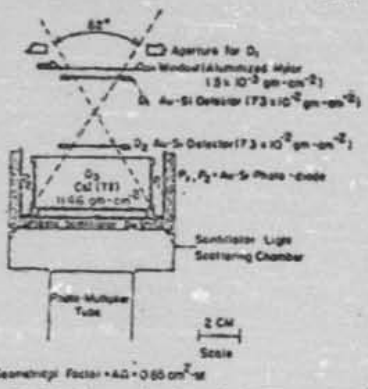

Fig. 2. Cross-section view of the detector elements and absorbers for the Imp 1 cosmic-ray telescope. Additional detector characteristics are given in Table 1. P_1 and P_2 are gold-silicon surface barrier photodiodes which detect the scintillation light from the CsI crystal. To initiate pulse height analysis the double coincidence D_1D_2 must be triggered. The depletion depths of detectors D_1 and D_2 are 200 microns.

D_1 and D_2. Detector D_3 is a CsI (Tl) crystal mounted inside a plastic scintillator cup, D_4. The light output from the D_3 scintillator is detected by two solid-state photodiodes (P_1, P_2) each having a photosensitive area of 2.5 cm². They are mounted on opposite sides of the CsI crystal.[3] Detection of the D_3 light by photodiodes eliminates the problem of coupling to photomultiplier tubes by a light-scattering chamber or light pipe, yet we obtain an energy resolution comparable to that of photomultiplier tubes for large energy losses. The signal outputs from P_1 and P_2 are summed in a mixer circuit. The scintillator cup D_4 detects any charged particle passing through the scintillator so that a charged particle escaping from D_3 or entering D_3 from the side will be recorded by a photomultiplier tube which is coupled to D_4 by a

[3] The photodiodes and their coupling to scintillators were developed in our laboratory. *Tarsolino et al.* [1962] have investigated the use of gold-silicon surface barrier detectors as photodiodes. *Fan* [1964] has examined their coupling efficiency and energy resolution with CsI scintillators.

TABLE 1. Characteristics of Imp 1 Charged-Particle Solid-State Telescope

Detector	Energy Threshold Sensitivity	Counting Rate Channels Determined by Particle Range (for protons), Mev	Geometrical Factor, cm² ster	Dynamic Ranges for Charged Particle Pulse Height Analysis
D_1	180 kev			
D_2	180 kev			
D_3	13 Mev			
D_4	300 kev			
D_5		0.9–190*	~3*	
D_1D_2 coincidence		6.5–190	0.85	
$D_1D_2D_3$ coincidence		19–190	0.85	
$D_1D_2D_3D_4$ coincidence		90–190	0.85	
Energy loss in D_3 (D_1D_2 coincidence)				High-gain range: 180 kev to 3 Mev Low-gain range: 3 to 35 Mev (see Figure 4)
Energy loss in D_4 ($D_1D_2D_3$ coincidence)				High-gain range: 15 to 200 Mev Low-gain range 360 Mev to 1.9 Gev (see Figure 5)

* Defined by aperture in Figure 2 for low energies.
Note: The response of detector D_5 for electrons is discussed by *Fan et al.* [1964b].

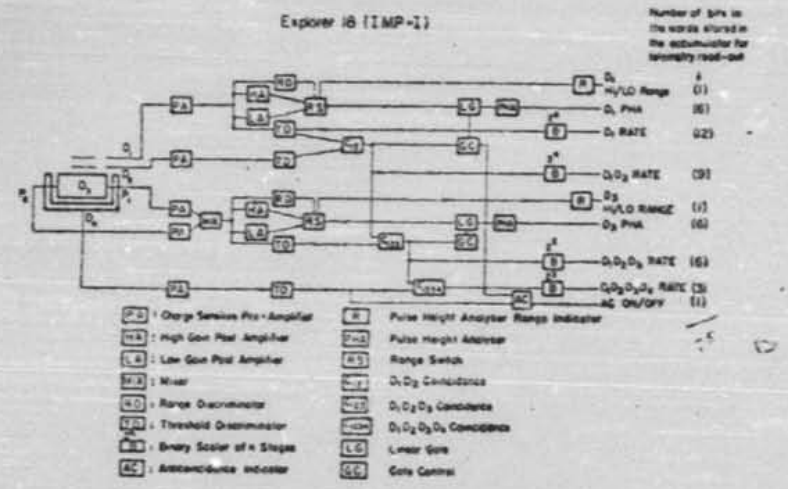

Fig 3. Electronics block diagram of principal logic functions. Note that the range switches place the D_3 and D_4 pulse height analyzers in either high-gain or low-gain modes as shown in Figures 4 and 5.

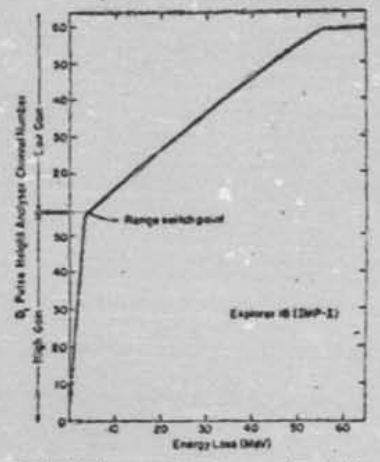

Fig. 4. Dual range calibration curve for the D_1 solid-state detector.

light-scattering chamber. To analyze an event, a charged particle must pass through D_1 and D_2 in coincidence, in which case a measurement of the energy loss is obtained in D_1. If the particle penetrates to D_2, an analysis of the pulse height in D_2 is also obtained, along with information about whether or not the particle penetrated into D_3.

Table 1 gives some additional characteristics of the telescope, the individual detectors, and their responses to particles in the telescope. The geometrical factor of the telescope is $0.85^{+0.02}_{-0.03}$ cm² ster.

Instrument electronics. Figure 3 is a block diagram indicating the principal logic elements in the instrument. It is important to note that each 64-channel pulse height analyzer on D_1 and D_2 independently has two dynamic ranges of operation so that large pulses from charged particles $Z \leq 6$ are analyzed. The calibrated pulse height ranges are given in Figure 4 for the D_1 analyzer, and in Figure 5 for the D_2 analyzer. The data from the analysis of a single event are stored in a 15-bit accumulator which is read-out on the average each 50 seconds and transmitted to the earth for data analysis. In addition, the counting rates of particles are divided according to particle range as shown in Table 1 and read-out on the average each ~50 seconds. For high flux levels the analysis channel *samples* the composition of particles, whereas the counting-rate channels measure the true flux of the incoming particles according to particle range in the telescope. With an over-all counting rate resolution of ~10 μsec, the dynamic range for flux measurements includes even large solar flares.

Detector energy resolution. The energy resolution of the D_1 and D_2 detectors and amplifiers was investigated in the laboratory. Three principal factors limit the resolution of D_1 for a vertically incident particle: the uniformity of depletion depth over the sensitive area of the

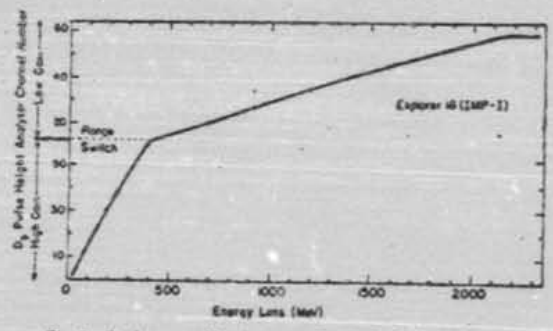

Fig. 5. Dual range calibration curve for the D_2 CsI scintillator.

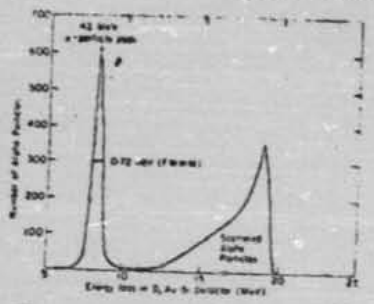

Fig. 6. Energy resolution for 42-Mev helium nuclei from the Argonne National Laboratory cyclotron. In addition to the direct beam there is a low-energy background distribution of helium nuclei whose cutoff at ~19-Mev energy loss provides an independent calibration of detector depletion depth.

detector; the Landau effect; and the noise from the charge-sensitive amplifier. The noise level of the detector and amplifier was equivalent to approximately 40 kev energy loss. Figure 6 shows the response of D_1 for 42-Mev α particles. The over-all resolution of D_1 is 720 kev full width at half maximum (FWHM) for vertically incident α particles. Since the sensitive area of the gold-silicon detectors extends slightly beyond the periphery of the gold deposit, owing to the fringe electric field, there exists a region whose area is <3% of the total area within which the charge collection drops to zero. In the coincidence mode D_1D_2 this effect only slightly downgrades the over-all resolution of D_1. Corrections for the Landau effect in D_2 become competitive with instrument resolution above ~50 Mev/nucleon for helium nuclei. The CsI-photodiode D_3 resolution for relativistic μ mesons and 40-Mev He^4 nuclei has been published [*Fan*, 1964, Figure 4]. With the amplifier outputs from P_1 and P_2 mixed as shown in Figure 3 to increase the signal-to-noise ratio by the factor 1.4 the over-all resolution is 17 to 35% (FWHM), depending on the total energy deposited in D_2.

Linearity of detector response for $1 \leq Z \leq 10$. We have investigated the response of the D_2 detector for both the amount of energy lost as a function of particle energy and for energy lost as a function of particle charge, Ze. The response to protons is linear over the entire energy loss range [*Stone*, 1964]. For $Z \geq 2$ the highest-energy particles available to us[a] in the laboratory in a beam with excellent energy resolution are limited to 10 Mev/nucleon. Since 10 Mev/nucleon particles of $Z \geq 7$ would end their range within the 200-micron depletion depth of D_2 we would be measuring the total energy loss in the depletion region diffusion and would not be taking into account the additional charge collected from beyond the depletion depth by diffusion [*Koch and Mesnier*, 1961]. Therefore it is essential to measure the energy lost by a particle passing completely through both the depletion and diffusion regions. To accomplish this we reduced the reverse bias potential on the D_2 detector so that the depth of the combined depletion and diffusion region was less than the particle range. In this way we measured the energy loss for H, He^4, He^3, C, O, and Ne nuclei at 10 Mev/nucleon energy. The linearity of response is demonstrated in Figure 7 for depletion depths of 68, 78, and 125 microns. The additional charge collection by diffusion may be interpreted as an increase in the depletion depth. From these measurements we find that the diffusion region in the D_2 gold-silicon detector is approximately 10% of the depletion depth.

It is well known that the scintillation light output from CsI is not linearly proportional to the energy lost in a crystal. However, for helium nuclei this correction is <3%.

Preflight and inflight calibrations. In addition to the detailed calibration of D_1 and D_2 detectors using accelerator particles, it was essential to provide periodic checks on the stability of the calibration throughout the preflight environmental testing, via vibration, vacuum, and thermal tests, and on the rocket before launch. This was accomplished by applying an external dc bias to disable all the coincidence circuits so that pulses from the individual D_1 and D_2 detectors could be analyzed by their respective pulse height analyzers without requiring a

[a] We wish to thank Dr. A. Ghiorso and the staff of the Lawrence Radiation Laboratory, University of California (Berkeley), for making available to us the Hilac accelerator and facilities for these studies.

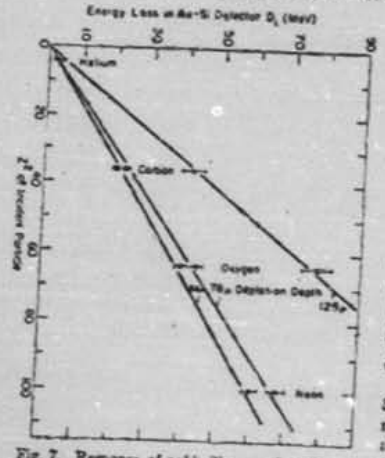

Fig. 7. Response of gold-silicon surface barrier detector D_1 to totally stripped nuclei of helium, carbon, oxygen, and neon from the Hilac accelerator at Berkeley. The energy of all particles was 10 Mev/nucleon. The measurements were made with amplifiers and circuits identical to those of Imp 1.

D_1D_2 or $D_1D_2D_3$ coincidence Am^{241} sources of α particles (5.5 Mev) were permanently mounted on thin Mylar foils over each detector. By introducing some absorption in mounting the source, the peaks of the energy distributions were brought into the high-gain ranges of Figures 4 and 5, while a few events in the high-energy tail fall into the low-gain ranges. Thus the peak channel number and range switch point could be checked by disabling the coincidence circuits. The Am^{241} α-particle intensity in D_1 was <0.1 count/sec, so that small fluxes in the D_1 counting-rate channel could be measured during flight. The entire instrument maintained its initial calibration over the 6-month period of preflight testing.

We have found that the helium data obtained in flight provide the best available calibration of the instrument after launch.

Stability. Within the temperature range $-10°$ to $+40°$C the maximum channel shift of the pulse height analyzers was <1.5 channels over the entire high-gain and low-gain ranges of D_1 (Figure 4) and the high-gain range of D_2 (Figure 5). The low-gain range of D_2 shifted by ~ 3 channels above channel 40. The thresholds for the counting-rate channels were constant within 5% over the above temperature range. In flight the satellite thermal control maintained a temperature of $\sim 20°$C with a maximum change of $<6°$C during the 5 months of data acquisition. Thus, no corrections for thermal effects were required, even in the passage through the shadow of the earth.

We found that the performance of all the solid-state detectors was satisfactory throughout the 5-month period, indicating that the detectors were not damaged in the radiation belts. This confirms experiments in our laboratory by Tuzzolino, Kristoff, and Perkins (unpublished) on gold-silicon surface barrier detectors.

In a study of the instrument behavior for the 5-month period after launch we found three malfunctions in electronic circuits, but fortunately none of them present problems for the analysis of our helium data. First, there was a gradual downward gain shift of $\sim 15\%$ in all high-gain mode channels of D_2 over the 5-month period; it was corrected in the analysis by the calibration of the instrument with the helium data. Second, at the time of launch there was an approximately 15-channel shift, confined to the low-gain mode of D_2. Third, after launch we found that a spurious background was observed that interferes with the analysis of the low-energy proton data; it is due to spurious pulses appearing in D_2 channel <15. This 'crosstalk' was not present before launch.

Although these shifts must be taken into account in the study of particles with $Z > 2$, and in the analysis of whether there is a significant helium component at very low energies, they do not affect the helium spectrum above 30 Mev/nucleon that we report in this paper.

Telescope orientation and orbital parameters. The main axis of our telescope was normal to the spin axis of the satellite. The cone of acceptance for particles excluded the solar paddles and included only the distant tip of the magnetometer boom, which has a negligible effect. Illustrations showing the Imp 1 spacecraft in flight configuration and the detailed projections of the satellite orbit in the ecliptic plane, and the variation of the sun-apogee angle and the solar aspect angle with time, are given by *Ness*

TABLE 2. Imp 1 (Explorer 18) Orbital Parameters

Launch date	Nov. 27, 1963, 0239:01.07 UT
Initial orbital period	93.5 hours = 3.89 days
Inclination to earth's equator	33.32°
Right ascension of ascending node	258.5°
Eccentricity	0.937
Initial apogee	197,616 km geocentric distance (~31 earth radii)
Initial perigee	192 km
Initial apogee sun angle	21.6°
Initial spin rate	22.27 rpm
Spin axis–satellite sun angle	111°
Right ascension of spin axis	116.6°
Declination of spin axis	−23.5°

Note: The satellite spends 66% of the orbital period at a distance beyond 20 earth radii.

et al. [1964]. In Table 2 we have summarized the orbital parameters for the spacecraft. Since the orbit is stationary in inertial space the apogee appears to rotate clockwise with respect to the sun-earth line at the rate of ~1° per day, as observed from the north pole of the sun.

The total weight of the instrument is 3.6 kg, and its total power requirement is <1 watt.

3. The Helium Spectrum and Flux

Data selection and analysis. We have sorted the pulse height data according to whether or not the particles penetrate into D_1. Those that do not penetrate are classified as anticoincidence 'off' events and are used to determine the primary helium spectrum. The data are gathered for all times when the instrument is outside the radiation belts. At the Goddard Space Flight Center symposium on the initial results of the Imp I satellite (unpublished 1964) we reported the appearance of recurring 27-day proton streams during the 3-month period, but we do not find detectable changes in the helium spectrum at these times in the energy range considered here. (G. Gloeckler, 'Solar modulation of the low-energy helium spectrum as observed on the Imp I satellite,' to be published.) Therefore, the only data we have excluded were for the period following the solar flare of March 16, 1964.

For a specific nuclear species with incident kinetic energy E entering at an angle θ with respect to the main axis of the telescope, we have computed the energy loss in D_1 and the total residual energy deposited in D_2, and converted them into appropriate channel numbers, taking account of both the known telescope absorbers in Figure 2 and calibrations discussed in section 2. Thus, for each kind of particle entering at angle θ we obtain a unique curve that we call a particle 'track' in a plane with the D_2 channel number as the abscissa and the D_1 channel number as the ordinate. For a range of θ from 0° to 30°, the distribution of individual tracks generates the areas shown in Figure 8 for He^4 and He^3 in the high-gain modes for both D_1 and D_2 pulse height analyzers. We have included a track for normally incident H^1 to illustrate the magnitude of separation of nuclear species. For the telescope geometry shown in Figure 2 the incremental contributions to the total geometrical factor are small for values of $\theta > 23°$ as shown in the appendix (Figure 12). Consequently, the main distribution of data points arising from angular spread of incident particles will lie well inside the boundaries shown in Figure 8. The additional effects of D_1 and D_2 detector resolution discussed in section 2 also contribute to the spread of data points. We find that the spread in our analyzed data agrees with our estimation of these effects, the discussion of which we defer to a later paper. They do not present a problem for the analysis of helium nuclei as long as we do not attempt to separate He^4 from He^3.

Some of the raw data from Imp 1 are superposed on the calculated curves in Figure 8, the distribution of points being plotted directly from an electronic computer in increments of channel number. The dependence of data point size on the number of events falling on the same coordinates of the $D_1 - D_2$ plane is described in the legend of Figure 8. We find that there is a clear separation of helium from hydrogen. The cross-talk events discussed in section 2 are found below D_2 channel 15 and primarily in the D_1 low-gain mode. Near the range switch point for D_2 the sample of helium events is obviously small and comparable to the background. Therefore, we have cut off our quantitative analysis at 30 Mev/nucleon for the results we report in this paper. The upper energy cutoff for analysis is determined by He^4 penetration into the D_2 detector at 90 Mev/nucleon. On the basis of

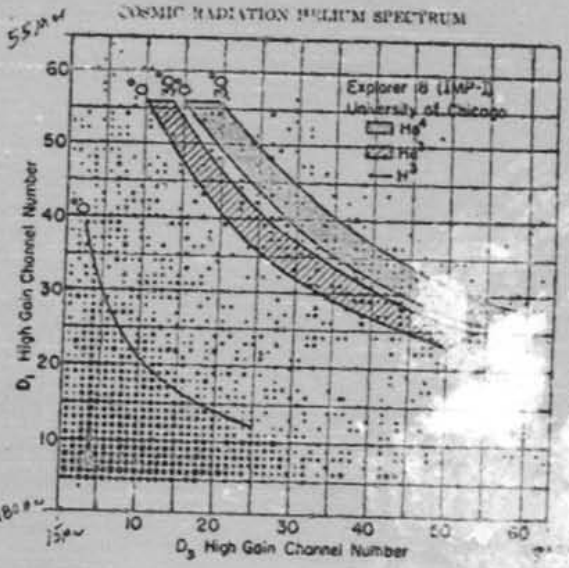

Fig. 8. The solid-line curves and enclosed areas identify the calculated tracks for helium nuclei and tritium based on the calibration curves and absorber distribution in the [illegible] particle telescope, Figure 2. The maximum angle of acceptance is 30°; 0° is for normal incidence. The data points represent raw data from 40 orbital periods. For display purposes the distribution of data points was plotted directly from an electronic computer in terms of channel number. The size of the dot is a measure of the number of events at that [illegible]. The smallest dot equals 1 event; the largest dot in the helium population is 8 events. The high density of events with D_1 channel ≤ 15 is mostly due to cross talk between D_1 and [illegible]

these selection procedures all the data reported here fall into the D_1 and D_2 high-gain mode.

Since the telemetry limits the analysis to only 1 event approximately every 50 seconds, we obtain a random sampling of the components in the cosmic radiation which preserves the relative charge abundances of the components. Thus, the number of helium events accumulated in the high-gain D_1-high-gain D_3 plane is not a measure of the helium flux, but it will depend on the relative abundance of helium with respect to all other analyzed components. Because of the relatively low abundance of helium with respect to all other possible analyzable events, and because of the low telemetry readout rate, the total number of helium nuclei in the energy range 120 to 360 Mev total kinetic energy accumulated in one orbital period was typically about 20. This requires an averaging of the data over 40 orbital periods to obtain the six-point spectrum reported in this paper.

The data were analyzed as follows: We first determined the helium track by using the *experimental* data to compute the mean D_1 channel number position for each D_3 channel number. A smooth curve was fitted to these points which represented the most likely 'center of gravity' of the helium population as a function of energy.

By selecting six energy intervals we obtained six frequency histograms of D_1 channel numbers. By assigning the D_1 channel track position the zero channel number, we obtained the relative channel number distributions shown in

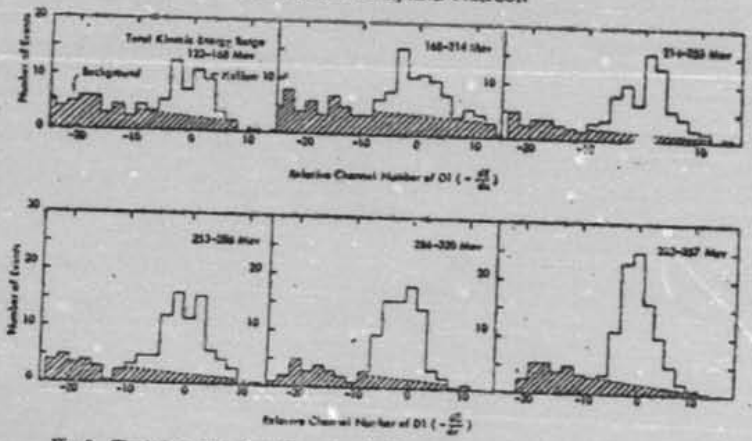

Fig. 9. The helium data for a 5-month period have been divided into six energy groups. The dashed line represents the interpolated background correction described in section 3. The helium nuclei in the energy range 320 to 357 Mev are all He^4, since all He^4 nuclei in this energy range penetrate the anticoincidence detector, D_5.

Figure 9. In these data we note the presence of some background, especially for the lowest energies, arising from low-energy nucleon disintegrations that do not trigger the D_1 scintillator. This background was subtracted from the helium distributions by computing running averages for each distribution. Although the averaging process tended to broaden the peak distributions, we were able to make background corrections reproducibly and unambiguously.

From the six distributions we obtain the six-point differential energy spectrum in Figure 10, using the fluxes calculated below.

We require information from the counting-rate channels D_1, D_2, D_3, D_4 to determine the flux of helium particles. The pulse height analysis data provide a ratio R_1 of the number of events in the helium population to the total number of events that did not trigger the D_1 detector. We obtain a second ratio, R_2, from the number of events that did not penetrate to the D_4 detector to the number of events penetrating the complete telescope, i.e., anticoincidence 'on' events. If we call the D_1, D_2, D_3, D_4 counting rate C, and the geometrical factor $A\Omega$, then

$$\text{Integral helium flux} = R_1R_2C/A\Omega$$

The Energy spectrum. The differential energy spectrum for the primary helium nuclei is shown in Figure 10 with error bars primarily due to the statistical uncertainty with which the individual points could be determined. Errors due to background subtraction and flux meas-

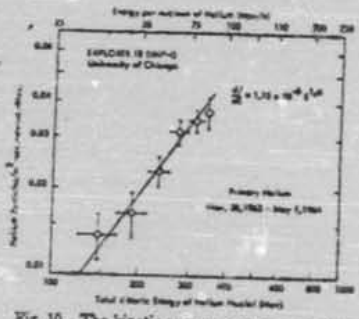

Fig. 10. The kinetic energy spectrum of helium (He^3 + He^4) nuclei. It is argued in section 4 that this is the modulated spectrum of helium from the nearby interstellar medium. Between 315 and 357 Mev only the flux of He^4 was measured.

urements are also included. We derive a power law dependence with an exponent of $+1.4 \pm 0.2$ for the spectrum by assuming a straight-line fit to the six points. The average differential helium flux in this energy range is ~0.03 helium nucleus/m² sec ster Mev. It is interesting to note that the anticoincidence 'cO' cutoff energy for He^3 is at 315 Mev but at 357 Mev for He^4. Consequently, the flux of 315–357 Mev helium nuclei in Figure 10 arises from He^4 only.

We pointed out that, at energies below 30 Mev/nucleon, background events made it difficult to determine the flux of helium. There is little doubt, however, that a substantial fraction of the analyzed events in the range 10 to 30 Mev/nucleon are helium nuclei.

The helium flux was continuously present over the 40 orbital periods from which the time-averaged spectrum in Figure 10 was derived. We find that the helium flux level over the energy range in Figure 10 increased by ~35% over the 5-month period. In this same time the increase in relativistic primary proton flux derived from neutron intensity monitor data as shown in Figure 1 was ~6%.

4. Origin of the Helium Nuclei and the Solar Modulation of Their Spectrums

Three facts convince us that the helium spectrum in Figure 10 is the modulated spectrum of interstellar helium nuclei and not a flux of solar origin. (1) This spectrum of helium nuclei was continually present over the entire period of measurement and not correlated with solar-flare phenomena. (2) The helium spectrum joins smoothly with the higher-energy helium spectrum obtained in balloon observations already identified as galactic radiation (for example, *Fichtel, Guss, Stevenson, and Waddington* [1964]; *Freier and Waddington* [1964]). In comparing these results in Figure 11, we made the reasonable assumption that the helium flux consists mostly of He^4, so that we may convert the energy spectrum to a magnetic rigidity spectrum since the balloon altitude observations

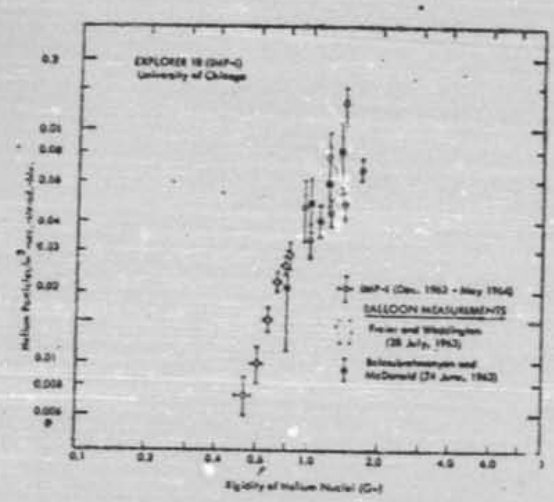

Fig. 11. The spectrum of helium nuclei as a function of magnetic rigidity. For comparison the published data at higher energies from balloon observations are shown. If we corrected the balloon data for time dependence due to solar modulation these data would represent the modulated spectrum prevailing near the 1964 minimum of the solar cycle.

were reported in units of magnetic rigidity. A better fit could be made if the changes in flux levels occurring over the time intervals of the various measurements arising from the 11-year solar modulation were taken into account. [3] From neutron intensity monitor measurements we deduce that the recovery of the relativistic proton flux from 11-year solar modulation shown in Figure 1 continues throughout the period, being approximately 6% in the 5-month interval over which the 30–60 Mev/nucleon helium flux increased by ~35%. Qualitatively, this is the expected behavior for the solar modulation of an interstellar spectrum, because the low energies are more strongly modulated than the high energies. [*Meyer and Simpson*, 1957; *Parker*, 1963]. The Imp 1 satellite measurements are consistent with the increase of low-energy ionizing radiation observed by *Neher* [1957] during periods of solar minimums.

Since the neutron monitor intensity—hence relativistic primary proton intensity—continued to increase above the level shown in Figure 1 beyond the period of the Imp 1 measurements, it is certain that the magnetic modulation region that was decaying beyond the earth's orbit was effective for modulating the low-energy helium spectrum at all times during the 5-month period. Therefore, the true interstellar spectrum of He^4 plus He^3 in the vicinity of our solar system should have an exponent substantially less than the +1.4 measured in Figure 10.

The proton spectrum was measured on Imp 1 by *McDonald and Ludwig* [1964] at the same time as our helium observations. Their 5-month, time-averaged spectrum is also approximated by a power law with exponent ~+1.5, over the same energy per nucleon interval; i.e., the protons and helium spectrums appear to have the same form of velocity spectrums. It is important, as was noted in the introduction, to determine whether or not there are relative differences in the time rate of change of the proton and helium spectrums during the decay phase of the solar modulation. This problem is now under investigation and will be reported later in a paper by Gloeckler, 'The time dependence of the low-energy helium spectrum.'

Since galactic helium nuclei down to 10 Mev/nucleon can reach the orbit of the earth near solar minimum, other particles of higher charge from the interstellar medium in this low-energy range also have access to the orbit of the earth at this time and are being measured.

Appendix

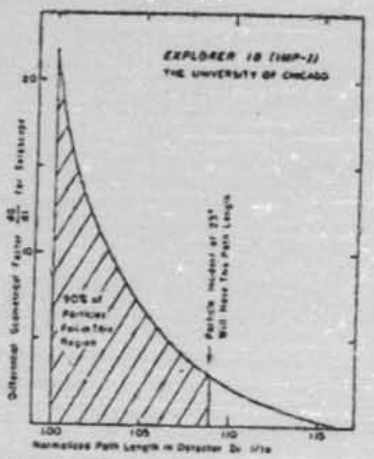

Fig. 12. The differential geometrical factor dG/dl for the telescope shown in Figure 2 as a function of normalized path length l/k, in the D_1 detector, where l is the path length of the charged particle in the sensitive region of the detector.

Acknowledgments. We are grateful to the staff at the Goddard Space Flight Center for the integration of our experiment into the Imp 1 satellite, its launching, and the processing of telemetry data. In particular, we thank Paul Butler, Frank McDonald, Norman Ness, Robert Martin, and their staffs.

Within our group we are most appreciative of the engineering and checkout of our instrument by Remi Jacquet, assisted by J. LeBlanc and the laboratory technical staff. The detector development work by A. Tuzzolino and his group was essential to the success of the experiment. The preparation of computer programs and data reduction for analysis were undertaken by G. Lenta, M. Case, and C. Schauf. We thank J. Lamport for his assistance on many technical and administrative problems.

We wish to thank the staff of the Argonne National Laboratory for providing us with the 42-Mev helium beam facilities, and Mr. J. O'Callaghan for assisting us in the calibration of the detectors.

This research was supported in part by the National Aeronautics and Space Administration grant

178-64 and NAS 5-2990, and by the Air Force Office of Scientific Research grant 63-23. The Imp 1 satellite has been designated Explorer 18.

References

Balasubrahmanyan, V. K., and F. B. McDonald, Solar modulation effects on the primary cosmic radiation near solar minimum, *J. Geophys. Res.*, *65*, 3269–3282, 1960.

Fan, C. Y., Detection of scintillation photons with photodiodes, *Rev. Sci. Instr.*, *30*, 158–163, 1959.

Fan, C. Y., G. Gloeckler, and J. A. Simpson, Initial results from the first interplanetary monitoring platform (Imp 1), *Trans. Am. Geophys. Union*, *45*(2), 367–369, 1964a.

Fan, C. Y., G. Gloeckler, and J. A. Simpson, Evidence for >20-kev electrons accelerated in the shock transition region beyond the earth's magnetosphere boundary, *Phys. Rev. Letters*, *13*, 149–153, 1964b.

Fan, C. Y., P. Meyer, and J. A. Simpson, Experiments on the eleven-year changes of cosmic-ray intensity using a space probe, *Phys. Rev. Letters*, *5*, 272–274, 1960.

Fichtel, C. E., D. E. Guss, D. A. Kniffen, and K. A. Neelakantan, Modulation of low-energy galactic cosmic-ray hydrogen and helium, *J. Geophys. Res.*, *69*, 3253–3256, 1964.

Fichtel, C. E., D. E. Guss, G. R. Stevenson, and C. J. Waddington, Cosmic-ray hydrogen and helium nuclei during a solar quiet time in July, 1961, *Phys. Rev.*, *138*, B618–627, 1964.

Forbush, S. E., Cosmic-ray intensity variations during two solar cycles, *J. Geophys. Res.*, *63*, 651–669, 1946.

Freier, P. S., and C. J. Waddington, Hydrogen and helium nuclei in the cosmic radiation, *Phys. Rev. Letters*, *13*, 108–109, 1964. (See also The helium nuclei of the primary cosmic radiation as studied over a solar cycle of activity, *Space Sci. Rev.*, to be published.)

Koth, I., and J. Mewissen, Nuclear method of measurement of diffusion length in *P-N* junctions, *IRE Trans. Nucl. Sci. NS-8*, 83–90, 1961.

McDonald, F. B., and G. H. Ludwig, Measurement of low-energy primary cosmic ray protons on Imp 1 satellite, *Phys. Rev. Letters*, *13*, 783–785, 1964.

McDonald, F. B., and W. R. Webber, A study of the rigidity and charge dependence of primary cosmic ray temporal variations, *Intern. Conf. Cosmic Rays and Earth Storms, J. Phys. Soc. Japan*, *17*, *Suppl. A-I*, 415–423, 1962.

Meyer, P., and J. A. Simpson, Changes in the low-energy particle cutoff and primary spectrum of cosmic rays, *Phys. Rev.*, *106*, 568–571, 1957.

Neher, H. V., Cosmic rays near the earth geomagnetic pole in the summers of 1955 and 1956, *Phys. Rev.*, *107*, 588–592, 1957.

Ness, N. F., C. S. Scearce, and J. B. Seek, Initial results of the Imp 1 magnetic field experiment, *J. Geophys. Res.*, *69*, 3531–3570, 1964.

Ormes, J., and W. R. Webber, Measurements of low-energy protons and α particles in the cosmic radiation, *Phys. Rev. Letters*, *13*, 106–108, 1964.

Parker, E. N., *Interplanetary Dynamical Processes*, Interscience Publishers, New York, 1963.

Simpson, J. A., The primary cosmic ray spectrum and the transition region between interplanetary and interstellar space, *Proc. Intern. Conf. Cosmic Rays (at Jaipur)*, *2*, 155–169, Bombay, 1964.

Stone, E. C., A measurement of the primary proton flux from 10 to 130 million electron volts, *J. Geophys. Res.*, *69*, 2039–2043, 1964.

Tarrolino, A. J., E. L. Hubbard, M. A. Perkins, and C. Y. Fan, Photoeffect in silicon surface barrier diode, *J. Appl. Phys.*, *33*, 148–153, 1962.

(Manuscript received March 18, 1965; revised April 26, 1965.)

64- 060A

IMP 2 EXPL 21

YEAR	NDAY	HR	MIN	SEC	MILLISEC
1964	334	~~34~~	~~33~~ 33	10	363
1965	027	~~04~~ 04	03	37	452

64- 060A

IMP 2 EXPL 21

D-1578

MIN	SEC	MILLI SEC
~~39~~		
~~28~~	10	363
03	37	452

FILE 0001 DEC 1031 C1 4824

0101	330010070201	070501010211	040106010700	010000000101	000000000000	030304
0149	330511041102	000000011773	000000003331	033333333333	330000000000	000000
0197	771177000000	327243022233	000000000035	000030000754	000000000002	000000
0245	333333333333	333333333333	000000000000	000000000000	000000000000	000000
0293	000000005555	327243154161	000000000012	000000000000	327243142166	000000
0341	777777777777	777777777777	777777777777	777777777777	000000000000	202763
0389	000000000000	000000000000	000000000000	000000000000	777777777777	777777
0437	000000000000	000000000000	000000000000	000000000000	000000020300	000000
0485	000000000000	000000000000	000000000000	000000000000	000000000330	000000
0533	300000000000	000000000000	000000000000	000000000000	000000000000	000000
0581	000000000000	000000000000	000000000000	000000000000	000000000000	000000
0629	333330000000	000300000000	000003000300	003333333000	000000000000	000000
0677	300000000000	000000000000	000003003000	000000000000	000000000000	000000
0725	333333333333	000000000000	000000000000	000000000000	000000000000	000000
0773	333333000000	000000000000	000000000000	000333333333	000000000000	000000
0821	000000000000	300000000000	000000000000	000000033333	000000000000	000000
0869	333333333333	333333333333	333333333333	000000000000	333333330000	000000
0917	040001000410	010000000000	000000000000	000330033000	333000004000	000000
0965	000000000301	000333000000	000000000000	030305001101	030200040637	000000
1013	000000000045	000000000775	033333000303	000000000000	000333000177	771177
1061	000000000000	000000000000	327713131315	000000000425	327713023355	000000
1109	000000000000	000000000000	000000033000	000000000000	000000000000	777777
1157	777777777777	777777777777	777777777777	777777777777	000000000000	333335
1205	000000040401	000000011773	000000000002	000000000000	000000000000	000000
1253	771177000000	327713251250	000000033315	000033333775	000000000004	000000
1301	000000000000	000000000000	000000000000	000000330000	327713371203	000000
1349	333333357435	327713131176	000000003015	000033033031	000033000301	203563
1397	777777777777	777777777777	777777777777	777777777777	777777777777	777777
1445	330004010510	000000155032	000630040402	000000011773	033333000303	000000
1493	000000000177	771177771177	771177000000	327715511135	000000000346	000000
1541	327713523131	000000000035	000333333036	000000000001	202431463145	203400
1589	000000000775	000000000007	000030007442	327713643064	000000000000	000000
1637	000000000000	777777777777	777777777777	777777777777	777777777777	777777
1685	000000000000	000000000000	000033333330	000000000000	002205040211	070501
1733	330033000000	030305001101	020333043337	000033166333	000600040400	000000
1781	300000000000	000000000000	000000033177	771177771177	771177000000	327713
1829	333333333333	000000007425	327713023321	000033033333	333300000000	000000
1877	327713131260	000000000045	000000000775	000333033033	000000007430	327713
1925	000030000000	000033300000	000000000000	777777777777	777777777777	777777
1973	777777777777	777777777777	000000000000	030305001101	030432021003	000001
2021	000030000002	000000000000	000000000000	000000000000	000000000177	771177
2069	000000000045	000033300775	000000000004	000000007433	327713263206	000000
2117	000000000000	000000000033	327713371146	000000003046	000000300775	000000
2165	000000000015	000003033001	000033333001	203563146315	400000000330	777777
2213	777777777777	777777777777	777777777777	777777777777	000000000000	030305
2261	330630040402	000000011773	000033033033	003330303000	000000000330	000330
2309	771177000000	327713511101	000000033046	000330000775	000000000006	000000
2357	330330000006	000000000001	202431463145	203403333030	327713631033	000000
2405	000330007442	327713643027	000000000000	000000033000	000000000001	000000
2453	777777777777	777777777777	777777777777	777777777777	777777777777	777777
2501	000030004000	000000000000	002205040211	070501010300	040001000410	010000
2549	330430100411	000330155334	000600043404	000330011771	003033000331	000000
2597	000000000177	771177771177	771177703016	327714210711	000000000046	000000
2645	327714322704	000000000171	300033333000	000000000000	211726000300	000000
2693	000000000776	000000000003	000030007454	327714342637	000000000000	000000
2741	330000000000	777777777777	777777777777	777777777777	777777777777	777777
2789	330000000000	030305001101	113311561134	000000166035	000600040405	000000
2837	330000000003	000000000000	000000003177	771177771177	771177000000	327714
2885	330000000003	000000007457	327714452572	000030033006	000000000000	000000
2933	327714575531	300000000047	000003003775	000330033034	333330007461	327714
2981	330333000000	202431463146	203400000000	777777777777	777777777777	777777
3029	777777777777	777777777777	000000000000	000330000000	003330000330	000000
3077	000333333333	330330333000	000000000000	000000303333	333333000000	000000

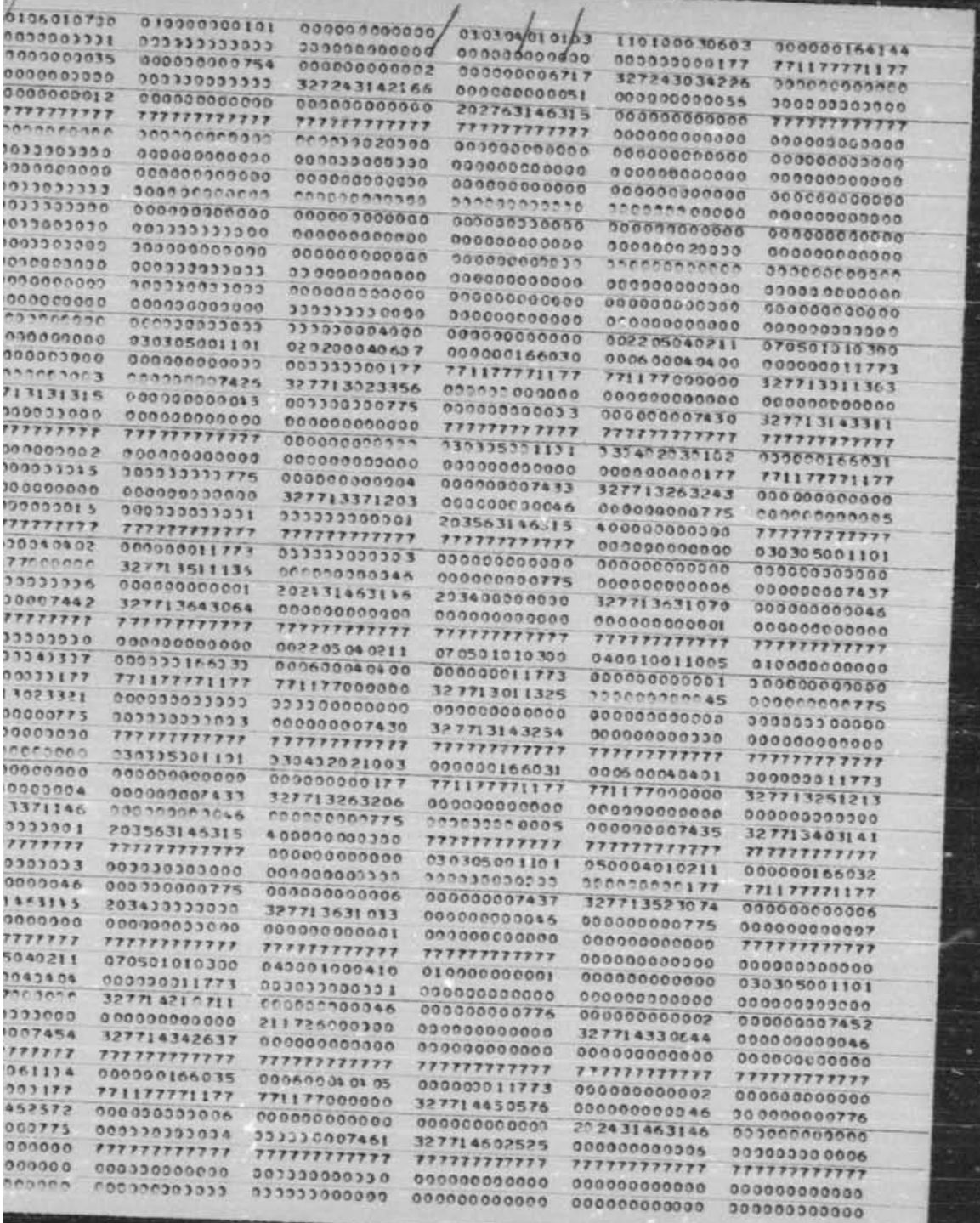

FILE 0001 REC 3011 CH 4824

3025	000000000000	000000000000	000000000000	000000000000	000000000000	000000000
3073	303000000000	000000000000	000000000000	000000000000	000000000000	000000000
3121	000000000000	000000000000	000000000000	000000000000	000000000000	000000000
3169	000000000000	000000000000	000000000000	000000000000	000000000000	000000000
3217	[illegible]	070501010300	040010011305	010000000000	000000000000	000000000
3265	330503040404	000000011773	000000000001	000000000000	000000000000	030305001
3313	771177000000	327714210654	000000000046	000000000776	000000000002	000000000
3361	[illegible]	[illegible]	211726000000	000000000000	327714330507	000000000
3409	000000007454	327714342602	000000000000	000000000000	000000000000	000000000
3457	777777777777	777777777777	777777777777	777777777777	777777777777	777777777
3505	110011060605	000001660035	030600040405	000000011773	000000000002	000000000
3553	000000000177	771177771177	771177000000	327714450541	000000000045	000000000
3601	327714462535	000000000006	000000000000	000000000000	202431463146	000000000
3649	000000000776	000000000001	000000007451	327714602467	000000000005	000000000
3697	000000000000	777777777777	777777777777	777777777777	777777777777	777777777
3745	000000000300	030305001102	000001050101	000000165036	000000040406	000000011
3793	000000000000	000000000000	000000000177	771177771177	771177000000	327714710
3841	[illegible]	[illegible]	327714723422	000000000000	000000000000	000000000
3889	327715030362	000000000047	000000000776	000000000005	000000007466	327715042
3937	000000000001	201643656051	202431463146	777777777777	777777777777	777777777
3985	777777777777	777777777777	[illegible]	[illegible]	[illegible]	[illegible]
4033	040001000410	010001010000	000000000000	000000000000	000000000300	000000000
4081	000000020000	000000000000	000000000000	000000000000	000000000300	000001660
4129	000000000000	000000000000	000000000000	000000000000	000000000300	000000000
4177	000000000000	000000000000	000000000000	000000000000	000000000000	000000000
4225	000000000000	000000006000	000000000000	000000000000	000000000000	000000000
4273	000000000000	000000000000	000000000000	000000000000	000000000000	000000000
4321	[illegible]	000000011773	000000000032	000000000000	000000000000	030305001
4369	771177000000	327715650125	000000000053	000000000776	000000000000	000000000
4417	000000000000	000000000001	201643656051	000000000000	000000000000	000000007
4465	[illegible]	327716[illegible]2053	000000000000	000000000000	327715770060	000000000
4513	777777777777	777777777777	777777777777	000000000000	000000000001	000000000
4561	050501010300	000000165042	000000040500	777777777777	777777777777	777777777
4609	000000000177	771177771177	771177000000	000000011773	000000000003	000000000
4657	327715122305	000000000025	000000000045	327716110012	000000000050	000000007
4705	000000000776	000000000002	000000007512	000000000001	204474631453	205543146
4753	000000000000	777777777777	777777777777	327716241741	000000000000	000000000
4801	000000000000	000000000000	000000000000	777777777777	777777777777	777777777

FILE 0001 REC 3002 CH 4824

3101	002205040211	070501010300	040010011305	010000000000	000000000000	030305001
3149	000000040410	000000011773	000000000001	000000000000	000000000000	000000000
3197	771177000000	327715410202	000000000050	000000000776	000000000006	000000007
3245	000000000010	000000000001	202503031303	203514631463	327715530135	000000000
3293	[illegible]	327715542130	000000000000	000000000000	000000000001	000000000
3341	777777777777	777777777777	777777777777	777777777777	777777777777	777777777
3389	040307000410	000000166041	000000040411	000000011773	000000000002	000000000
3437	[illegible]	771177771177	771177000000	327715530070	000000000050	000000007
3485	327715662063	000000000004	000000000000	000000000001	201643656051	000000000
3533	000000000776	000000000001	000000007505	327715002015	000000000000	000000000
3581	000000000000	777777777777	777777777777	777777777777	777777777777	777777777
3629	000000000000	030305001102	050501010103	000000165042	000000040500	000000011
3677	000000000000	000000000000	000000000177	771177771177	771177000000	327716107
3725	000000000001	000000007513	327715121751	000000000026	000000000045	000000000
3773	327716227710	000000000050	000000000776	000000000002	000000007512	327716241
3821	000000000001	000000000000	000000000000	777777777777	777777777777	777777777
3869	777777777777	777777777777	000000000000	000000000000	000000004000	000000000
3917	[illegible]	[illegible]	000000000000	030305001102	103402060104	000000156
3965	000000000001	000000000000	000000000000	000000000000	000000000177	771177771
4013	000000000351	000000007777	000000000004	000000007523	327715521561	000000000
4061	000000000000	[illegible]	327716727520	000000000051	000000000777	000000000
4109	000000000004	000000000032	000000001001	201643656051	201763146315	777777777
4157	777777777777	777777777777	777777777777	777777777777	000000000000	030305001

000000000000	000000000000	000000000000	000000000000	000000000000	000000000000
000000000000	000000000000	000000000000	000000000000	000000000000	000000000000
000000000000	000000000000	000000000000	000000000000	000000000000	000000000000
000000000000	000000000000	000000000000	000000000000	000000000000	000000000000
040010011005	010000000000	000000000000	010305001101	070007100200	000000166034
000000000001	000000000000	000000000000	000000000000	000000000177	771177771177
000000000046	000000000776	000000000002	000000207452	327714222647	000000000171
211726000000	000000000000	327714330607	000000000046	000000000775	000000000003
000000000000	000000000000	000000000000	000000000000	000000000000	777777777777
777777777777	777777777777	777777777777	777777777777	000000000000	030305001101
000600040405	000000011773	000000000002	000000000000	000000000000	000000000000
771177000000	327714450541	000000000045	000000000776	000000000003	000000007457
000000000000	000000000000	202431463146	000000000000	327714570474	000000000047
000000007451	327714602467	000000000005	000000000026	000000000000	202431463146
777777777777	777777777777	777777777777	777777777777	777777777777	777777777777
000301051101	000000165036	000600040406	000000011773	000000000303	000000000000
000000000177	771177771177	771177000000	327714710427	000000000047	000000000776
327714722422	000000000000	000000000000	000000000000	000000000000	000000000000
000000000776	000000000005	000000007466	327715042355	000000000004	000000000003
202431463146	777777777777	777777777777	777777777777	777777777777	777777777777
000000003000	000300000000	000000004000	000000000000	002205040211	070501010300
000000000000	000000000000	000000000000	000000166040	000000000000	000000000000
000000000000	000000000000	000000000000	000000000000	000000000000	000000000000
000000000000	000000000000	000000000000	000000000000	000000000000	000000000000
000000000000	000000000000	000000000000	000000000000	000000000000	000000000000
000000000000	000000100000	000000000000	000000000000	000000000000	000000000000
000000000000	300000000000	000000000000	030305001102	040307000707	000000166041
000000000032	000000000000	000000000000	000000000000	000000000177	771177771177
000000000053	000000000776	000000000000	000000007503	327715562120	000000000004
201643655051	000000000000	327715770060	000000000050	000000000775	000000000001
000000000000	000000000000	000000000001	000000000000	000000000000	777777777777
777777777777	777777777777	777777777777	777777777777	000000000000	030305001102
000600040500	000000011773	000000000003	000000000000	000000000000	000000000000
771177000000	327716110012	000000000050	000000000776	000000000001	000000007510
000000000045	000000000001	204474531453	205543146315	327716227745	000000000050
000000007512	327716241741	000000000000	000000000000	000000000001	000000000000
777777777777	777777777777	777777777777	777777777777	777777777777	777777777777
000000000000	000000000000				

040010011005	010000000000	000000000000	030305001102	030105020002	00000016604[illegible]
000000000001	000000000000	000000000000	000000000000	000000000177	771177771177
000000000050	000000000776	000000000006	000000007476	327715422175	000000000010
202500000000	203514631463	327715530135	000000000052	000000000776	000000000007
000000000000	000000000000	000000000001	000000000000	000000000000	777777777777
777777777777	777777777777	777777777777	777777777777	000000000000	030305001102
000600040411	000000011773	000000000002	000000000000	000000000000	000000000000
771177000000	327715553070	000000000050	000000000775	000000000000	000000007503
000000000000	000000000001	201543656051	000000000000	327715770022	000000000050
000000007505	327715002015	000000000000	000000000000	000000000001	000000000000
777777777777	777777777777	777777777777	777777777777	777777777777	777777777777
050510101103	000000155042	000500040500	000000011773	000000000003	000000000000
000000000177	771177771177	771177000000	327716107755	000000000050	000000000776
327715121751	000000000026	000000000045	000000000001	204474631463	205543146315
000000000776	000000000002	000000007512	327716241703	000000000000	000000000000
000000000000	777777777777	777777777777	777777777777	777777777777	777777777777
000000000000	000000000000	000000004000	000000000000	002205040211	070501010300
000000000000	030305001102	100402060104	000000156044	000500040502	000000011773
000000000000	000000000003	000000000177	771177771177	771177000000	327716607566
000000000004	000000007520	327716521561	000000000000	000000000000	000000000001
327716727520	000100000051	000000000777	000000000005	000000007823	327716741514
000000000001	201643655051	201763146315	777777777777	777777777777	777777777777
777777777777	777777777777	000000000000	030305001103	000004040511	000000165045